Applied Catalysis B: Environmental 148–149 (2014) 446–465

Contents lists available at ScienceDirect

Applied Catalysis B: Environmental

journal homepage: www.elsevier.com/locate/apcatb

Combined IR spectroscopy and kinetic modeling of NO_x storage and NO oxidation on Fe-BEA SCR catalysts

Stavros A. Skarlis[a,b], David Berthout[a], André Nicolle[a,*], Christophe Dujardin[b], Pascal Granger[b]

[a] IFP Energies Nouvelles, 1 et 4 avenue de Bois-Préau, 92852 Rueil-Malmaison Cedex, France
[b] Unité de Catalyse et de Chimie du Solide, UMR CNRS 8181, Université Lille 1, Sciences et Technologies, 59655 Villeneuve d'Ascq, France

ARTICLE INFO

Article history:
Received 1 August 2013
Received in revised form 9 November 2013
Accepted 13 November 2013
Available online 21 November 2013

Keywords:
NO_x TPD
Fe-BEA zeolite
IR spectroscopy
Kinetic modeling
Selective catalytic reduction.

ABSTRACT

A multi-site kinetic model for NO_x adsorption/desorption and NO to NO_2 oxidation on Fe-BEA was developed, based on *in-situ* IR spectroscopic measurements. NO and NO_2 adsorption, along with NO/O_2 co-adsorption were initially investigated on H- and Fe-BEA lab-synthesized samples, in order to elucidate the contribution of acidic and iron sites. Simultaneously an *in-situ* IR spectroscopic study allowed to characterize a variety of NO_x adspecies, including iron nitrosyls, nitrosium anions, nitrites as well as aluminum and iron based nitrates. Based on recorded spectral features a multi-site kinetic model for NO_x storage and NO oxidation was developed, accounting for interactions of nitrogen oxides with different surface sites. The model was finally validated, through simulation of various experimental conditions, depicting satisfactorily mechanistic aspects related to NO_x storage and NO oxidation on acidic and metallic sites.

1. Introduction

The selective catalytic reduction (SCR) of nitrogen oxides (NO_x) through urea or ammonia is currently recognized as the predominant technology for nitrogen oxides (NO_x) emissions control of mobile diesel engines. Among available catalytic formulations, iron exchanged BEA zeolites are considered as promising candidates for SCR applications under lean conditions [1,2].

The reduction of NO_x over Fe-zeolites is performed through a complex reactions network, which involves disproportionation of NO_2 towards nitrite/nitrate adspecies and subsequent interactions of the latter with chemisorbed ammonia, yielding nitrogen and water [3,4]. NO and NO_2 adsorption and desorption are reaction steps of particular interest in order to understand the SCR chemistry over Fe-exchanged zeolites. Numerous experimental studies reported in the recent literature tend to conclude that nitrite/nitrate adspecies, formed upon NO_2 adsorption and disproportionation are involved in reaction pathways through which the Fast-SCR occurs [5–7]. Furthermore, NO oxidation is supposed to be a crucial reaction step in the course of the SCR of NO_x on Fe-exchanged zeolites. Oxidation of nitric oxide leads to the formation of surface NO_2, which is considered as the initial step of standard SCR reaction [4,8].

NO_x adsorption and desorption over iron exchanged BEA zeolites is experimentally investigated in several studies. Colombo et al. [9] have performed series of NO_2 adsorption and TPD experiments over commercial Fe-BEA catalysts (Si/Al = 24, Fe/Al = 1.5) of different redox states, in order to elucidate the role of Fe^{2+} and Fe^{3+} species in NO_2 storage and disproportionation. Iwasaki and Shinjoh [10] correlated the abovementioned reactions with iron sites, employing FTIR measurements over Fe-zeolites, synthesized by different methods. Moreover, Shwan et al. [11] have presented NO adsorption and TPD experiments over fresh and aged Fe-BEA catalysts (1 wt.% Fe, SAR = 38) underlying the effect of hydrothermal ageing on iron sites oxidation state. A detailed IR spectroscopic study of Ahrens et al. [12], performed during NO_x adsorption on a 0.76 wt.% Fe-BEA catalyst (Si/Al = 40), allowed to unravel mechanistic aspects related to NO_2 disproportionation and nitrates formation over acidic and redox sites. These authors, as well as Kefirov et al. [13] have also investigated NO oxidation to NO_2 on Fe-BEA, enabling to elucidate the contribution of isolated and/or binuclear iron species on this reaction. Even though the discussed studies provide convincing arguments related to the role of iron active sites on NO_x storage and NO oxidation, the respective role of Fe-BEA acidity seems to remain unclear. Moreover, the thermal stability of NO_x adspecies has only been investigated through gaseous NO_x-TPD profiles [9,11]. However, the respective results have not been further validated through surface characterization.

Regarding the kinetic modeling of NO_x adsorption/desorption and NO oxidation over metal exchanged zeolites, several

* Corresponding author. Tel.: +33 0 147526688.
E-mail address: andre.nicolle@ifpen.fr (A. Nicolle).

0926-3373/$ – see front matter © 2013 Elsevier B.V. All rights reserved.
http://dx.doi.org/10.1016/j.apcatb.2013.11.018

Nomenclature

$A_{i,j}$: pre-exponential factor of the ith reaction on the jth surface site ($m^3/s\,kg_{zeolite}$)
A_{open}: single wafer reactor inlet port cross section (m^2)
CSTR: continuously stirred reactor
D_i: internal diameter of the fixed bed reactor (m)
EfAl: extra-framework aluminum
$E_{i,j}$ (θ,T_s): activation energy of the ith reaction on the jth surface site (J/mol)
$E_{0-i,j}$: activation energy of the ith reaction on the jth surface site for surface coverage equal to zero (J/mol)
FAl: framework aluminum
$k_{i,j}$: rate constant of the ith reaction on the jth surface site (1/s)
L_{bed}: length of catalyst particles bed (m)
$\dot{m}_g$: gas mass flow rate (kg/s)
P_{in}, P_{out}: gas absolute pressure at the inlet and outlet of the single wafer reactor (Pa)
R: global gas constant (8.314 J/(mol K))
SAR: silica to alumina ratio (–)
STPD: stepwise temperature programmed desorption
T_s: solid phase temperature (K)

Greek symbols
α_j: constant for the description of the dependence of the activation energy of desorption from the j site surface coverage (–)
θ_j: surface coverage of the jth catalytic site (–)
μ: dynamic viscosity ((N s)/m^2)
ρ_g: density of gas mixture (kg/m^3)

approaches have been presented in the bibliography. Metkar et al. [14] have modeled NO_2 adsorption and NO oxidation over Fe-ZSM5, employing a single iron site. A detailed reactions mechanism was adopted including NO_2 adsorption and disproportionation as well as NO oxidation by surface oxygen. Shwan et al. [11] described the adsorption of NO through a dual-site kinetic model, including one Brønsted type acidic site and one monomeric iron site. These authors have also proposed NO oxidation through gas phase interactions between NO and O_2. Bacher et al. [15] suggested a Langmuir–Hinshelwood type reaction rate expression to model NO oxidation, which accounts for inhibiting effects of H_2O and NO_2. Interestingly, Olsson et al. [16] have proposed a multi-site kinetic model for nitrates formation over Cu-exchanged ZSM5 catalysts, suggesting an initial NO_2 adsorption on (i) non acidic, (ii) Brønsted type acidic and (iii) copper sites, followed by disproportionation, exclusively occurring over the metallic ones. Finally, Colombo et al. [17] succeeded in modeling NO_2 storage and NO_3 formation on a single site, corresponding to redox copper sites of a commercial Cu-zeolite. Among the presented kinetic models, only those developed by Shwan et al. [11], Olsson et al. [16] and Colombo et al. [17] account for interactions of NO_x with acidic and metallic sites. Nevertheless, in the kinetic model proposed by Shwan et al. [11] NO oxidation was modeled in the gas phase and the redox cycle was not depicted. On the other hand, Olsson et al. [16] and Colombo et al. [17] have validated NO_2 adsorption and NO oxidation kinetic models over Cu-ZSM5 catalysts, whereas a multi-site approach has never been attempted over Fe-BEA catalysts.

In the light of the abovementioned discussion, it seems obvious that NO_x storage and disproportionation, as well as NO oxidation over Fe-BEA catalysts have been extensively investigated. Nevertheless, up to now the role of the zeolitic acidity has not been completely understood, whereas NO_x adspecies thermal stability is still under debate. Thus, in this work, dedicated NO and NO_2 adsorption and TPD experiments on both H- and Fe-exchanged BEA catalysts are presented. Employing *in-situ* IR spectroscopy, NO_x adspecies were characterized in details, enabling a deep insight into the contribution of catalyst acidity as well as redox properties.

Regarding kinetic modeling, the multi-site kinetic model suggested by Olsson et al. [16] is the only reported approach, which allows depicting NO_2 storage and NO oxidation over different sites of Cu-ZSM5 catalysts. On the other hand, such modeling approaches have not been attempted on Fe-zeolites (except from the model of Shwan et al. [11]). Hence, in this study, a multi-site kinetic model was developed on the basis of IR spectroscopic measurements, performed on the H- and Fe-BEA samples. The proposed model was validated by simulating NO_2 adsorption and TPD as well as NO oxidation experiments performed over the lab-synthesized catalysts and respective catalytic samples reported in the literature.

Table 1
Elemental analysis of the studied Fe-BEA catalyst.

Element	Composition (wt.%)	Molar amount [a] ($mol/kg_{Fe\text{-}BEA}$)
Fe	1.75	0.31
Al	2.98	1.11
Si	36.93	13.15

[a] Values computed by multiplying species mass composition with the respective species molar weight.

2. Experimental

A 1.75 wt.% Fe-BEA (Fe/Al = 0.28) catalyst (Table 1) was synthesized from an H type BEA zeolite (Si/Al = 11.8), applying wet ion exchange. Upon synthesis, the Fe-BEA sample was calcined in air, for 5 h, at 500 °C. Details about the synthesis and post-treatment of the sample as well as the respective physicochemical characterization can be found in our previous work [18].

Separate NO and NO_2 adsorption/desorption, as well as NO/O_2 co-adsorption were investigated on the H- and Fe-BEA catalysts. 10 mg of each sample were pressed into self-supported wafers of 2 cm^2 and placed in a single wafer reactor. The latter was installed in an electric oven so as to perform thermo-desorption experiments. Solid phase temperature was continuously measured through a k-type thermocouple, whereas mass flow controllers (Brooks Instrument) were employed in order to manage the feed gas composition.

NO storage and release were studied on the Fe-BEA catalyst, by preadsorbing 0.3% NO diluted in He for 100 min, at 30 °C. The sample was subsequently flushed with He for 1 h at the same temperature and a TPD was performed up to 485 °C, under He, applying a temperature ramp of 10 °C/min. Then, NO_2 adsorption and desorption experiments were performed on both the H- and Fe-BEA samples. A mixture of 0.45% NO_2, 8% O_2 and He in balance were introduced into the single wafer reactor at 30 °C for 100 min. Then, the samples were purged with He for 1 h, followed by a TPD up to 485 °C, at a rate of 10 °C/min. Finally, NO oxidation was studied over the Fe-BEA, by continuously exposing the catalyst to a mixture of 1100 ppm NO, 2% O_2 and He in balance. Simultaneously, the reactor temperature was stepwisely increased from 100 to 485 °C. Initially, the temperature was kept at 100 °C for 60 min, and then increased to constant steps of 150, 250, 300, 450, 485 °C. The duration of each step was 10 min, whereas the heating rate between the steps was 10 °C/min.

NO_x surface species were characterized by means of *in-situ* FTIR spectroscopy, employing a Nicolet 6700 spectrometer (resolution: 4 cm^{-1}, 64 scans recorded per spectrum). Simultaneously, a Nicolet 380 FTIR spectrometer (resolution: 1 cm^{-1}, 64 scans per spectrum)

was placed downstream the reactor in order to measure gaseous species concentrations.

All the abovementioned experiments were performed at atmospheric pressure, with a total gas flow rate of 10 standard cm^3/min. In order to ensure that the recorded IR spectra were not affected by surface impurities and/or residual amounts of NO_x adspecies, fresh catalytic samples were used for every experiment. Finally, before testing, each sample was activated at 400 °C, overnight, under He.

3. Modeling

3.1. Reactor models

Zero-dimensional models of a single wafer, a monolith and a fixed bed reactor were developed and implemented into the simulation environment LMS.Imagine.Lab AMESim [19]. The single wafer reactor was considered as a single continuous stirred tank (CSTR) and the respective model is presented in [18]. The monolith reactor was represented as a series of CSTRs, as described in our earlier work [20]. The fixed bed was modeled based on the approach previously adopted by Leistner et al. [21]. The reactor was considered as an open cylinder, containing particles of the Fe-exchanged zeolite. The working medium flows through the bed and the pressure drop is computed through the Darcy law:

$$P_{in} - P_{out} = \frac{\dot{m}_g \cdot \mu \cdot L_{bed}}{\rho_g \cdot A_{open}} \quad (1)$$

where L_{bed} and A_{open} correspond to the bed length and the reactor internal cross section area, respectively. The latter is calculated as follows:

$$A_{open} = \frac{\pi \cdot D_i^2}{4} \quad (2)$$

Fixed bed reactors can be described as a single, or a series of CSTRs, since the bed length is usually very thin (typically <1 mm) [21]. According to the computation of low Péclet numbers, the fixed bed was considered as a series of two tanks, assuming homogeneous temperature, pressure and species concentrations throughout the control volume. Mass and heat transfer within gas and solid phase were taken into account, by means of a Thiele modulus approach and 0-D heat balances, respectively. The complete set of equations has been presented in references [20,22].

3.2. Kinetic model

A multi-site kinetic model was developed on the basis of IR spectroscopic measurements over the lab-synthesized H- and Fe-BEA samples. Reaction rate expressions (Table S1, Supplementary Material) were formulated in line with the ones reported by Olsson et al. [16], who previously proposed a multi-site kinetic model for NO_x storage and NO oxidation over Cu-ZSM5. Reaction rate constants were described employing the Arrhenius expression.

$$k_{i,j} = A_{i,j} \cdot \exp\left(\frac{-E_{i,j}}{R \cdot T_s}\right) \quad (3)$$

As far as NO_2 desorption rate expression is concerned, it was judged essential to account for surface coverage dependent activation energies. Surface coverage dependency factors α (Table S1, Supplementary Material) reflect the dispersion and thus heterogeneity of surface sites, with respect to their acidic and/or redox properties [21]. As explained in detail in our previous work [18], Fe-BEA Brønsted acidity, as well as metallic sites Lewis type acidity strength are strongly dependent on the local environment of the respective positions of protonated OH^+ and Fe species in the zeolitic framework.

Table 2
Summary of NO_x adspecies observed during NO adsorption over the Fe-BEA lab-synthesized sample.

Adspecies	IR band (cm^{-1})	References
NO^+	2133	[23,24]
N_2O_3	1913	[24]
$(Fe\text{-}NO)^{2+}$	1874	[24]
Trans-$(NO)_2$	1767	[24]
Bridging Al based NO_3	1653	[24]
Adsorbed H_2O	1624	[25]
Bidentate Al based NO_3	1594	[24]
Chelating Al based NO_3	1580	[24,25]

4. Results and discussion

4.1. In-situ IR spectroscopy measurements

In-situ IR spectroscopic measurements, performed in parallel to NO, NO_2 adsorption and NO/O_2 co-adsorption on the H- and Fe-BEA lab-synthesized samples are presented in this section. The scope of this study is to characterize nitrogen monoxide adspecies formed on acidic and metallic sites, in order to elucidate their contribution to NO_x storage and NO oxidation.

4.1.1. NO adsorption and desorption on Fe-BEA

Nitrogen monoxide storage and release were studied through a NO adsorption and TPD experiment, performed over the Fe-BEA catalyst. Gas phase results are illustrated in Fig. 1. Overall, a limited NO uptake of 0.22 $mol/kg_{Fe\text{-}BEA}$ was estimated during the adsorption phase. Minor NO storage over Fe-exchanged zeolites has been also reported elsewhere [6,23]. The same amount was desorbed during the subsequent TPD experiment, whereas neither N_2 nor NO_2, nor N_2O were detected.

The nature of surface sites contributing to NO storage was elucidated through difference IR spectra recorded during the adsorption phase. Spectral features discussed in this section are summarized in Table 2. Regarding the OH region (Fig. S1—Supplementary Material), several IR minima were identified, which are discussed in our earlier work [18]. A negative IR band centered at 3782 cm^{-1} was assigned to the consumption of terminal Al–OH groups (framework Al-FAl), which exhibit basic or Lewis acidic properties. Moreover, bands lying at 3741 and 3665 cm^{-1} were related to interactions of NO with non acidic terminal silanols (Si–OH) and hydroxyl bonded to extra-framework aluminum (EfAl), respectively. A negative band at 3610 cm^{-1} was attributed to consumption of $Si\text{–}OH^+\text{–}Al$ Brønsted acidic sites. Finally, a decrease in intensity was observed at 3685 cm^{-1} and was assigned to the consumption of Fe^{3+}–OH [13].

Parallel to those observations, several IR bands were observable in the 2300–1400 cm^{-1} region (Fig. 2). After 10 min of NO exposure, corresponding to the Fe-BEA saturation phase (Fig. 2A), IR maxima centered at 2133 and 1874 cm^{-1} were identified and were attributed to nitrosium ion (NO^+) and $(Fe\text{–}NO)^{2+}$ mono-nitrosyl, respectively [24]. Hadjiivanov et al. suggested formation of NO^+ through interactions of NO with Brønsted acidic sites [23], leading to the formation of adsorbed H_2O and NO^+ coordinated to framework oxygen. Moreover, Kefirov et al. [13] proposed interaction of NO with Fe^{3+}–OH forming Fe^{2+} and HNO_2. Subsequent surface reaction of the latter with cationic OH^+ sites can yield NO^+ on lattice oxygen and H_2O. Indeed, in the presented experiment the 2133 cm^{-1} IR band arose along with a broad band at 1624 cm^{-1}, which can be assigned to adsorbed H_2O [25]. Moreover, negative IR bands at 3610 and 3685 cm^{-1} were evidenced, which correspond to zeolitic OH^+ and Fe^{3+}–OH, respectively. Therefore, both the abovementioned mechanisms could take place in the present experiment. At this stage it is worthwhile to be point out that the

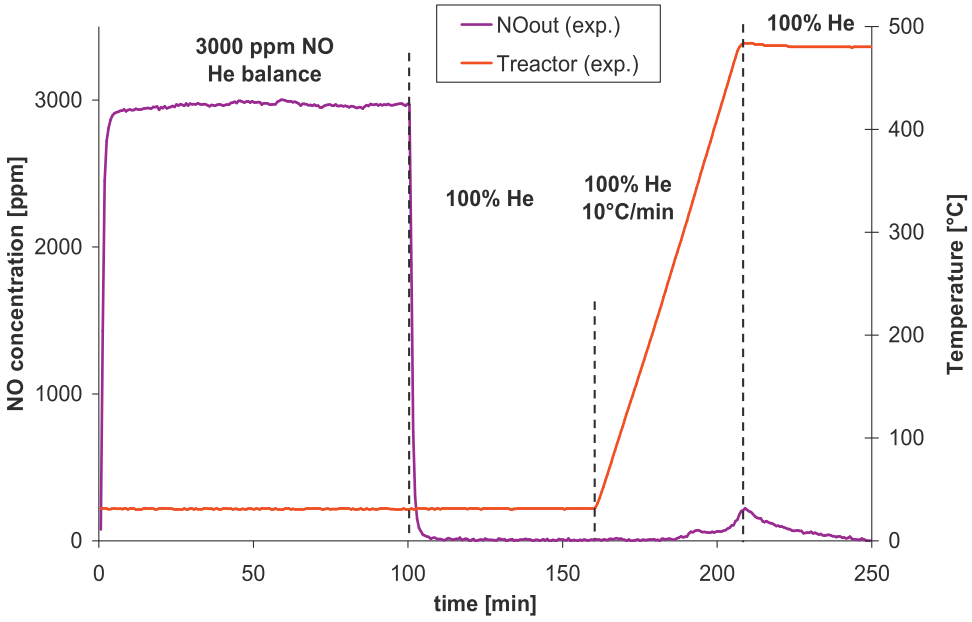

Fig. 1. NO adsorption and desorption experiments over the Fe-BEA studied catalyst: Preadsorption of 3000 ppm in He, for 100 min at 30 °C, followed by 60 min He flushing at the same temperature and TPD up to 480 °C at a heating rate of 10 °C/min.

existence of $(Fe–NO)^{2+}$ species may indicate that residual amounts of Fe^{2+} may exist on the Fe-BEA lab-synthesized sample.

Weak IR bands at 1913 and 1767 cm^{-1} were attributed to dinitrogen trioxide (N_2O_3) and trans-$(NO)_2$ dimer, which coexist in equilibrium with NO at low temperatures [24]. Finally, IR maxima at 1653 and 1580 cm^{-1} were assigned to bridging and chelating nitrate adspecies (NO_3), respectively [24,25]. Increasing exposure time (Fig. 2B), leads to the growth of the 1653 cm^{-1} IR band and the disappearance of the one lying at 1580 cm^{-1}. Simultaneously another band arose at 1594 cm^{-1} and was related to bidentate nitrates [24]. Based on several experimental studies, nitrates are formed on Fe-exchanged zeolites upon NO_2 adsorption and successive disproportionation [6,7]. However, the presented NO adsorption experiment was performed in the absence of oxygen. In such conditions no significant NO oxidation to NO_2 should occur. Hence, the observation of nitrates may involve reaction pathways irrelevant to NO_2 formation. Interaction of NO with zeolitic lattice oxygen may explain nitrates formation. Sedlmair et al. observed formation of monodentate NO_3 (1580 cm^{-1}) on EfAl, upon NO admission on NaY (Si/Al = 2.59) [25]. This assumption is likely to be supported for the studied Fe-BEA sample, since a negative bands centered at 3782 and 3665 cm^{-1} were observed, being assigned to FAl and EfAl.

Compiling information obtained through IR spectroscopic measurements, it can be concluded that NO preferably adsorbs on Brønsted acidic and Fe^{2+} monomeric sites. Moreover, interactions between Fe^{3+}–OH and NO likely occur. Finally, formation of NO_3 adspecies seems plausible through interactions of NO with lattice oxygen, possibly included in Al positions. These observations are summarized through reactions (R.1) to (R.5).

$$NO_{(g)} + 2H^+ - OZ \rightleftharpoons NO^+ - OZ + HO - H^+ - Z \quad \text{(R.1)}$$

$$NO_{(g)} + HO - Fe^{3+} - Z \rightleftharpoons HNO_2 - Fe^{2+} - Z \quad \text{(R.2)}$$

$$HNO_2 + H^+ - OZ \rightleftharpoons NO^+ - OZ + H_2O - Z \quad \text{(R.3)}$$

$$NO_{(g)} + Fe^{2+} - Z \rightleftharpoons [NO - Fe]^{2+} - Z \quad \text{(R.4)}$$

$$NO_{(g)} 2O - Al - Z \rightleftharpoons Z - Al - O - (NO) - O - Al - Z \quad \text{(R.5)}$$

4.1.2. NO_2 adsorption and desorption

4.1.2.1. In-situ IR spectroscopy measurements on H-BEA. NO_2 adsorption/desorption were studied first on the bare H-BEA zeolite, in order to evaluate the respective contribution of zeolitic acidic sites. Outlet gaseous NO and NO_2 concentration profiles recorded during NO_2/O_2 co-adsorption are shown in Fig. 3. 1.64 $mol/kg_{zeolite}$ NO_2 were stored on the H-BEA zeolite. Upon 2.5 min of NO_2/O_2 uptake, zeolite active sites for adsorption started becoming saturated and a weak NO concentration peak arose, which was associated to NO_2 disproportionation [6,7]. NO concentration was maximized at 4.5 min (ca 519 ppm) and then gradually attenuated without becoming zero, indicating that NO_2 adsorption and disproportionation reach equilibrium [26]. The ratio between the amounts of consumed NO_2 and produced NO, upon the saturation point, was estimated equal to 3 ($N_{NO2\_consumed}$ = 1.53 $mol/kg_{zeolite}$, $N_{NO\_produced}$ = 0.55 $mol/kg_{zeolite}$), which corresponds to the stoichiometry of reaction (R.6). Nevertheless, this estimation must be considered only as approximate since as it going to be discussed later (i) at 30 °C, NO_2 physisorption and/or weak adsorption may also take place, leading to an increase NO_2 uptake and (ii) interactions between NO and NO_2 may simultaneously occur.

$$3NO_2 + 1/2O_2 \rightleftharpoons 2NO_3 + NO_{(g)} \quad \text{(R.6)}$$

Difference IR spectra recorded during NO_2/O_2 introduction are collected in Fig. 4 and respective spectral features are summarized in Table 3. Regarding the first 10 min of the adsorption, three distinguishable negative IR maxima were observed in the OH-region (Fig. S2—Supplementary Material), centered at 3782, 3745 (including a component at 3741 cm^{-1}) and 3665 cm^{-1}. Surface sites corresponding to these IR bands have already been discussed in Section 4.1.1. Moreover, broad IR maxima appeared at ca 2900 and 2400 cm^{-1} and were ascribed to the bending and stretching modes of OH groups, respectively [27].

Simultaneously, several IR bands were observed in the 2300-1400 cm^{-1} region, which were assigned to different NO_x adspecies (Fig. 4). Focusing on the 2–10 min interval (Fig. 4A), intense IR maxima arose at 1653 and 1592 cm^{-1}, which were assigned to bridging and bidentate nitrates (NO_3), respectively (Section 4.1.1). Furthermore, weak IR bands were observed at 2133 and 2175 cm^{-1}. The

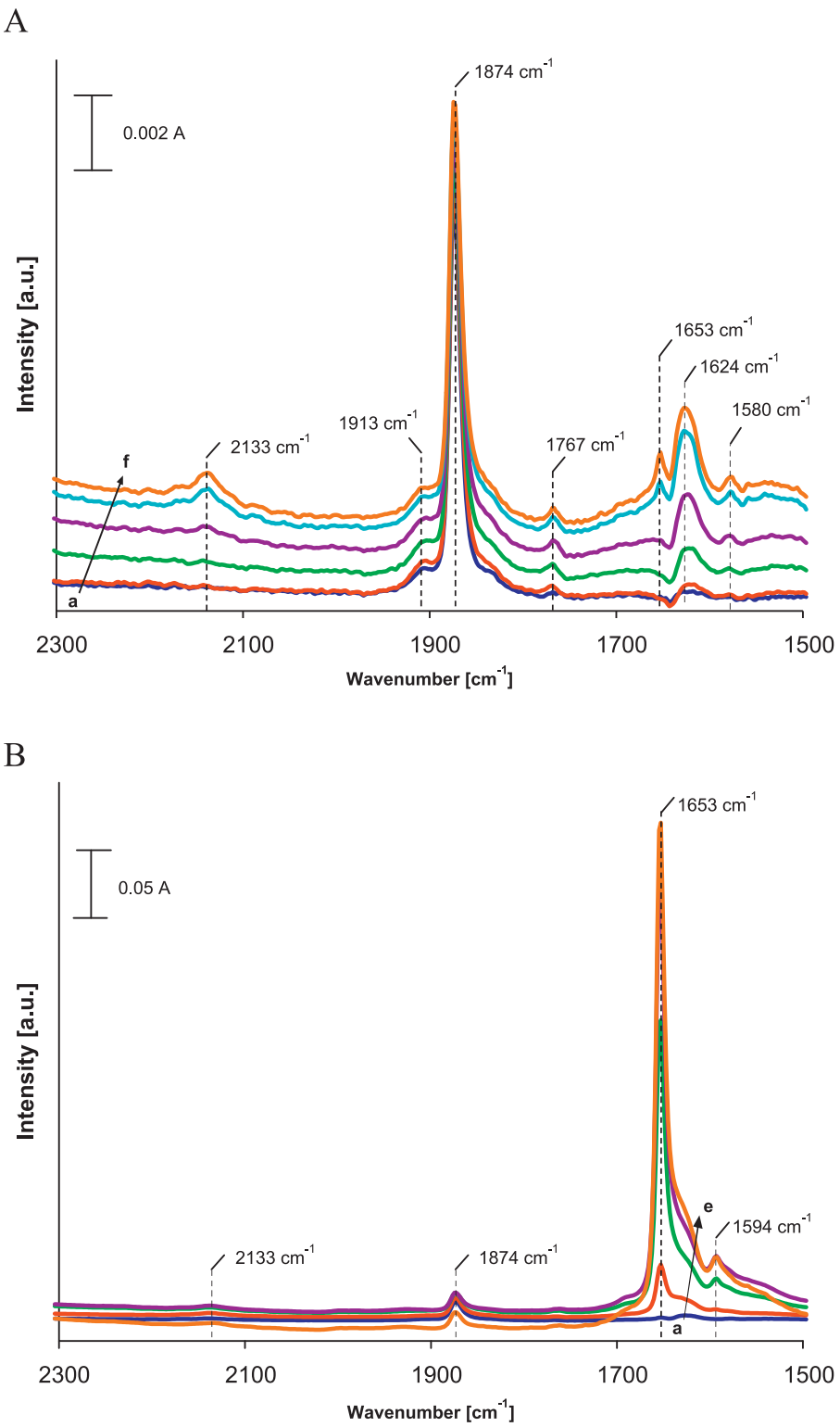

Fig. 2. Difference IR spectra recorded during NO adsorption over the Fe-BEA studied sample at 30 °C (injection of 3000 ppm NO in He). (A) Lines correspond to IR spectra recorded at: (a) 1 min, (b) 3 min, (c) 5 min, (d) 7 min, (e) 9 min and (f) 10 min. (B) Lines correspond to IR spectra recorded at: (a) 10 min, (b) 20 min, (c) 40 min, (d) 60 min and (e) 100 min.

former was attributed to the nitrosium ion NO^+ (Section 4.1.1), whereas the nature of the latter is quite unclear. Hadjiivanov et al. [23] reported that the 2200–2100 cm^{-1} range is related to several adspecies, including N_2O, NO_2^+ and NO^+. Elsewhere, it was assigned to N_2O_4 species [28], combined with an IR component centered at 1750 cm^{-1} [12]. Moreover, an IR band of increasing intensity was observed at 1743 cm^{-1} and was attributed to N_2O_4 species [27,29]. N_2O_4 formation is suggested either through NO_2 dimerization, or N_2O_3 oxidation [27]. The latter compound was evidenced via the IR band centered at 1865 cm^{-1}, and may originate from an interaction between NO and NO_2 [10,27]. The N_2O_4 dimer has been previously suggested as an intermediate species of the NO_2 disproportionation

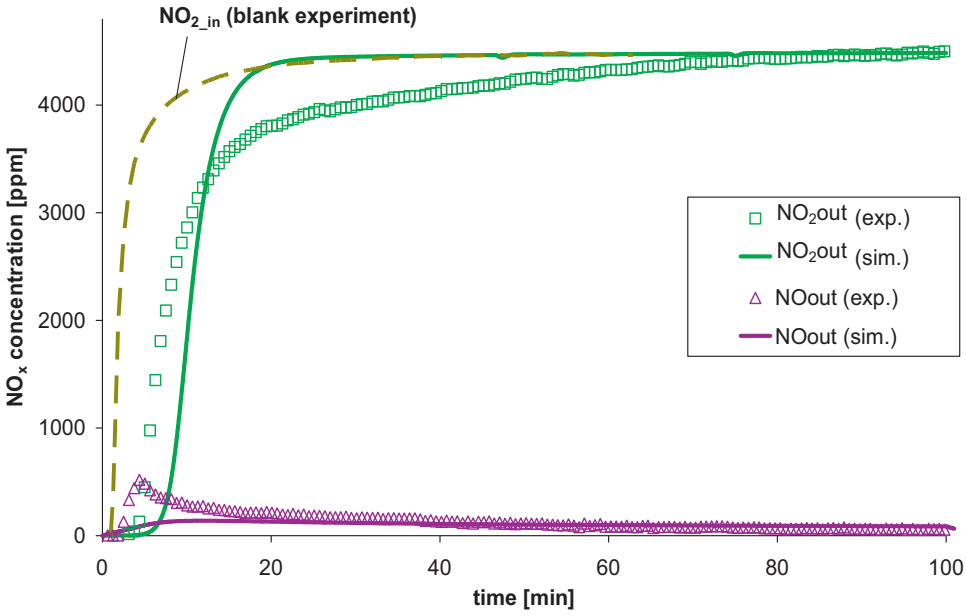

Fig. 3. Gaseous NO_x concentrations recorded during NO_2 storage on the lab-synthesized H-BEA zeolite at 30 °C. (Injection of 0.45% NO_2, 8% O_2 and He in balance for 100 min).

Table 3
Summary of NO_x adspecies observed during NO_2 adsorption over the H-BEA lab-synthesized sample.

Adspecies	IR band (cm^{-1})	References
N_2O, N_2, NO_2^+	2175	[24]
N_2O_4		[28]
NO^+	2133	[23,24]
N_2O_3	1865	[24,27]
Trans-$(NO)_2$	1767	[24]
N_2O_4	1743	[27,29]
NO_2	1675	[31]
Bridging Al based NO_3^-	1653	[24]
Bridging Al based NO_3^-	1628	[12,24]
Adsorbed H_2O	1624	[25]
Bidentate Al based NO_3^-	1592	[24]
Chelate nitrite	1517	[24]

process [6,30] (reaction (R.7)). Elsewhere, the 1743 cm^{-1} IR band was assigned to weakly sorbed N_2O_4 [27,29].

$$2NO_2 \rightleftharpoons N_2O_4 \rightleftharpoons NO_3^- + NO^+ \quad \text{(R.7)}$$

Increasing exposure time ($t > 2$ min: Fig. 4B) the 2133 and 2175 cm^{-1} IR bands vanished, whereas that related to bridging NO_3 (1653 cm^{-1}) remained quasi unchanged. Simultaneously, IR maxima centered at 1675 and 1517 cm^{-1} arose and were assigned to weakly adsorbed nitro groups (asymmetric bending mode of NO_2) [31] and chelating nitrite [24] adspecies, respectively. Finally, a broad IR band was identified at 1630 cm^{-1}, gradually shifting to 1624 cm^{-1}. The interpretation of this band is not obvious. According to the literature, a 1628 cm^{-1} IR band may correspond to bridging Al based NO_3 [12,24], whereas adsorbed water was related to a band centered at 1624 cm^{-1} (Section 4.1.1). Apostolescu et al. [32] suggested NO_3 formation accompanied by gaseous NO release, through a sequential mechanism involving interactions between NO^+ and gaseous NO_2, according to reactions (R8) and (R9).

$$NO^+ + O^{2-} \rightleftharpoons NO_2^- \quad \text{(R.8)}$$

$$NO_2^- + NO_{2(g)} \rightleftharpoons NO_3^- + NO_{(g)} \quad \text{(R.9)}$$

The sum of reactions (R.7)–(R.9) leads to reaction (R.6), discussed above.

In order to further elucidate the nature of surface sites contributing to NO_2 disproportionation, normalized intensity profiles of IR maxima observed in the OH and ON region were compared (Fig. 5). A maximum intensity was observed for the 2133 and 1653 cm^{-1} IR bands at ca 2.5 min, which is in excellent agreement with gas phase results (Fig. 3). This comparison indicates the occurrence of NO_2 disproportionation yielding NO_3 (1653 cm^{-1}) and NO^+ (2133 cm^{-1}). Profiles of the 1653 and 3782 cm^{-1} bands were somehow symmetric, suggesting that bridging NO_3^- was formed on terminal Al–OH, which exhibits Lewis type acidity or basicity. A similar behavior was identified for the 2133 and 3610 cm^{-1} profiles, which seems to indicate occupation of Si–OH^+–Al Brønsted sites by NO^+, according to the mechanism discussed in Section 4.1.1. Finally, normalized intensities of IR peaks lying at 1592 and 3665 cm^{-1}, exhibited relative symmetry. Thus, it could be suggested that bidentate NO_3 were formed on EfAl.

The abovementioned results imply that NO_2 disproportionation involved both FAl and EfAl (thus a Lewis acidic sites) for NO_3 formation and framework oxygen, generated upon interaction of Si–OH^+–Al Brønsted acidic sites with NO. IR studies of NO/O_2 co-adsorption on H-MOR [33] and Na-Y [25], as well as DFT calculations of N_2O_4 disproportionation on alkali exchanged X [34] and Y [35] zeolites somehow validate this conclusion. However, if we accept the heterolytic chemisorption of NO_2, close vicinity between Lewis and Brønsted sites is prerequisite. Indeed, Wang et al. have confirmed this conclusion for H-MOR zeolites, highlighting the existence of attractive interaction between the aluminum coordinated NO_3 and a neighboring OH^+ cation [33].

The thermal stability of the discussed NO_x adspecies was evaluated through a 1 h He purging at 30 °C followed by a TPD experiment, illustrated in Fig. 6. Respective IR spectra are presented in Fig. 7. Overall, around 1.64 $mol/kg_{zeolite}$ NO_2 were desorbed, in line with the respective amount of nitrogen dioxide stored during the adsorption phase. At 100 °C, an intense NO_2 gaseous concentration peak, along with a weak NO peak were observed. As clearly shown in Fig. 7A, upon the 1 h He purging at 30 °C, the IR peak at 1743 cm^{-1} vanished completely. Therefore, it can be suggested that the 1743 cm^{-1} band is likely related to weakly sorbed N_2O_4. Interestingly, a short desorption delay was evidenced up to 50 °C, whereas above 75 °C all IR maxima in the ON region attenuated.

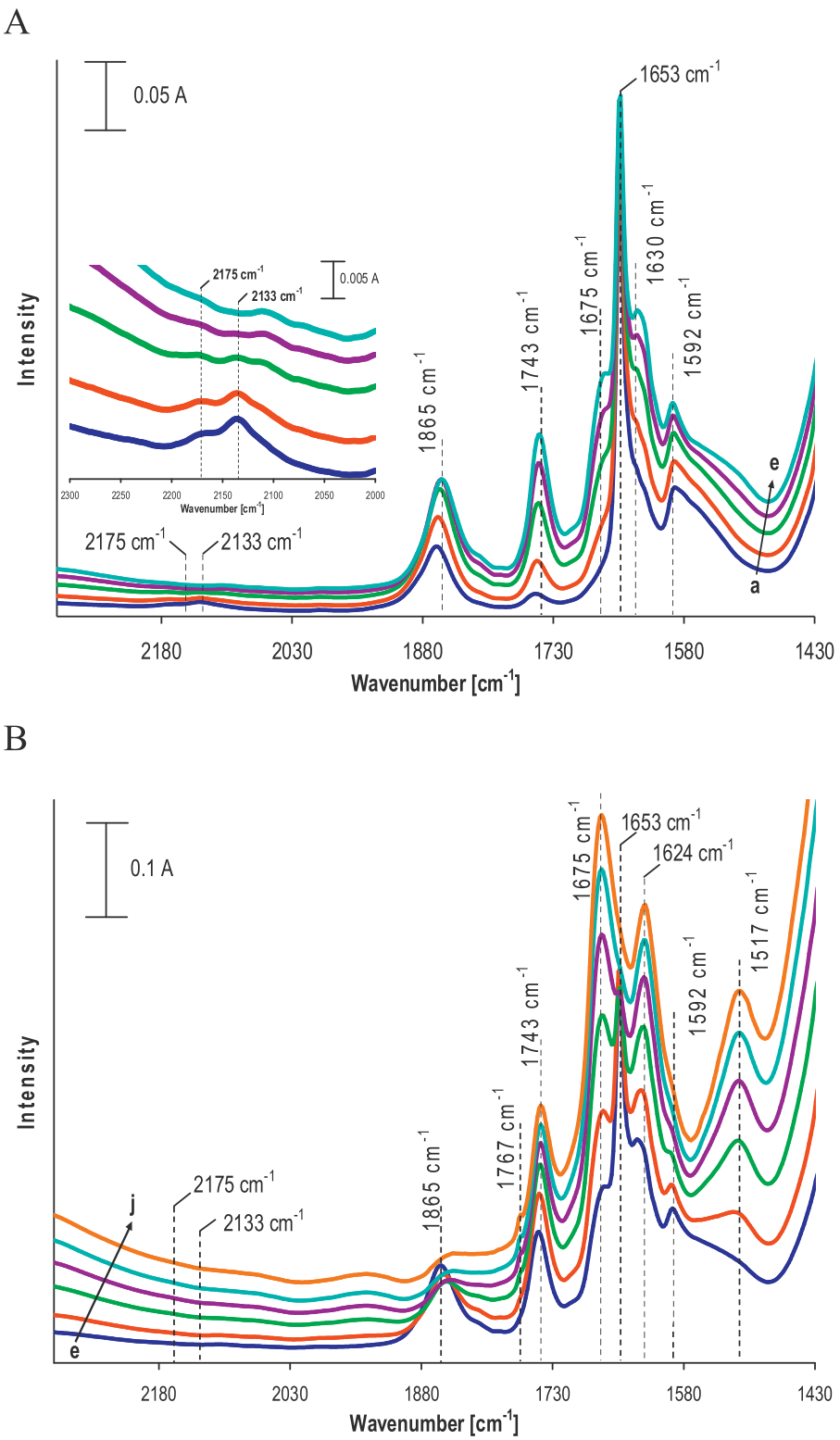

Fig. 4. Difference IR spectra recorded during NO_2 adsorption over the H-BEA zeolite at: (a) t = 2 min, (b) t = 4 min, (c) t = 6 min, (d) t = 8 min, (e) t = 10 min, (f) t = 20 min, (g) t = 40 min, (h) t = 60 min, (i) t = 80 min, (j) t = 100 min. (Injection of a mixture of 0.45% NO_2 and 8% O_2 dilluted in He, at 30 °C, during 100 min).

Among them, the contribution at 1767 cm^{-1} disappeared. Hence small amounts of NO desorbed at the same temperature range were attributed to removal of weakly bonded (*trans*-$(NO)_2$). Finally, evacuating the sample at 100 °C, the 1675, and 1518 cm^{-1} IR bands, related to nitrites disappeared. Therefore, the NO_2-TPD peak at 100 °C was assigned to NO_2 desorbed from non-acidic sites and/or sites for weak adsorption, as well as to NO_2 deriving from nitrite adspecies.

As far as the high temperature regime is concerned (Fig. 7B), only nitrates were observed. Upon evacuation at 250 °C, bidentate NO_3 were eliminated (1592 cm^{-1}), whereas at 300 °C bridging nitrates were removed (1653 cm^{-1}). Therefore, we concluded that

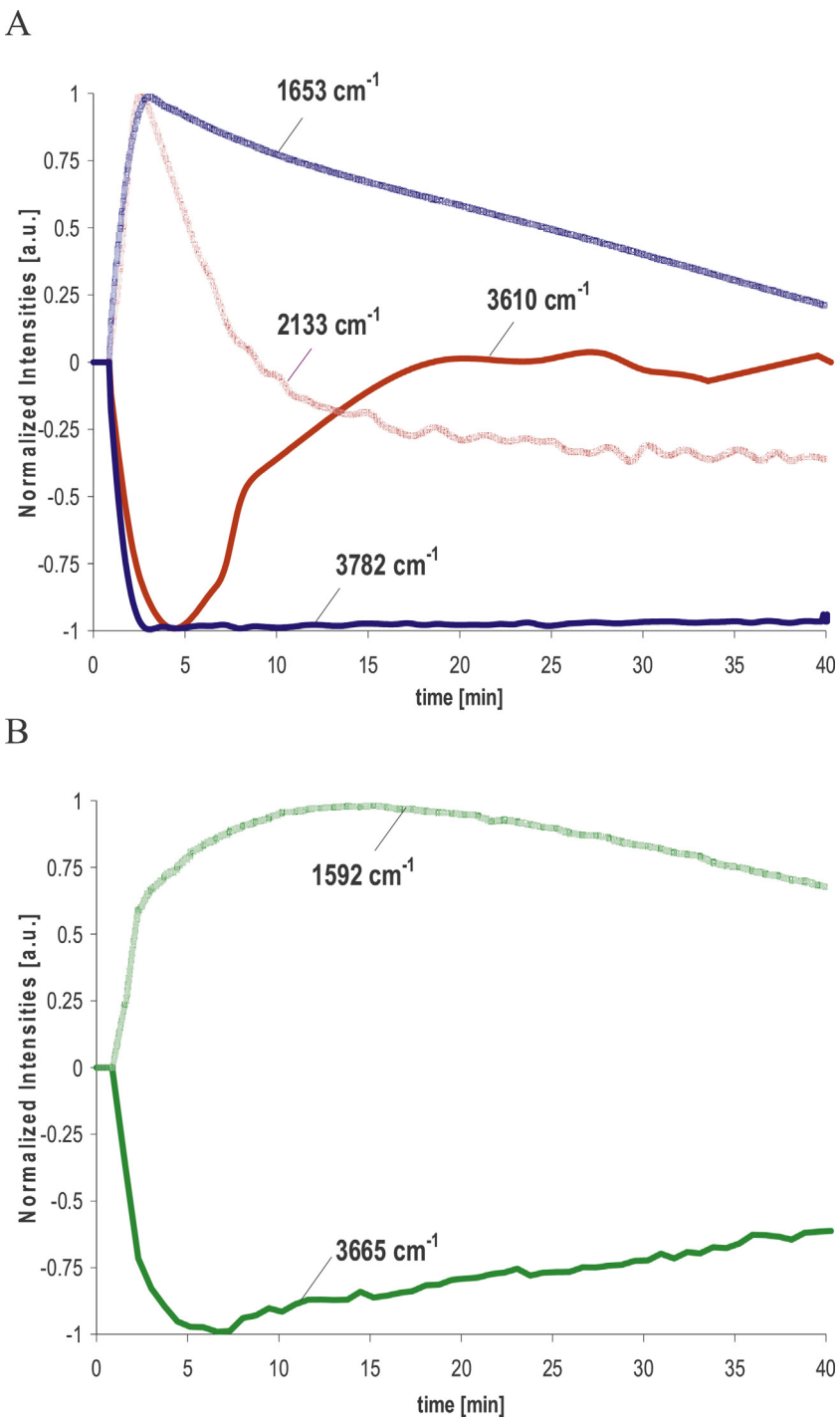

Fig. 5. Normalized intensity of the peaks associated with NO_2 disproportionation. Normalization was performed at maximum or minimum peak intensity for each of the presented IR bands, according to the methodology reported elsewhere [10].

the broad NO_2-TPD peak at around 210 °C and the shoulder at 250 °C were related to NO_2 mainly deriving from decomposition of bidentate NO_3 (1592 cm^{-1}), whereas the NO_2-TPD shoulder at $T > 300$ °C was assigned to gaseous NO_2 generated after decomposition of bridging NO_3.

Interestingly, above 300 °C, NO breakthrough was observed which was previously assigned to NO_2 dissociation on Brønsted sites [16]. Earlier it was shown that NO_3 is formed on FAl and EfAl, Lewis type acidic sites, in vicinity with a Brønsted type one. Therefore, a decomposition of NO_3 to NO_2 and a dissociation of the latter on a neighboring OH^+ cannot be excluded. Moreover, decomposition of gaseous NO_2 to NO at such high temperatures could also be possible.

4.1.2.2. In-situ IR spectroscopy measurements on Fe-BEA. The effect of the Fe-BEA iron species on NO_2 adsorption and desorption was studied through an additional NO_2 adsorption and TPD experiment, performed on the Fe-exchanged BEA at 30 °C. Gaseous concentration profiles recorded during NO_2/O_2 adsorption on Fe-BEA are shown in Fig. 8. 1.44 mol/$kg_{Fe\text{-}BEA}$ NO_2 were stored on the catalyst. The surface became saturated upon ca 4.5 min of NO_2/O_2 introduction, whereas NO started to evolve at around 1.8 min. The amounts

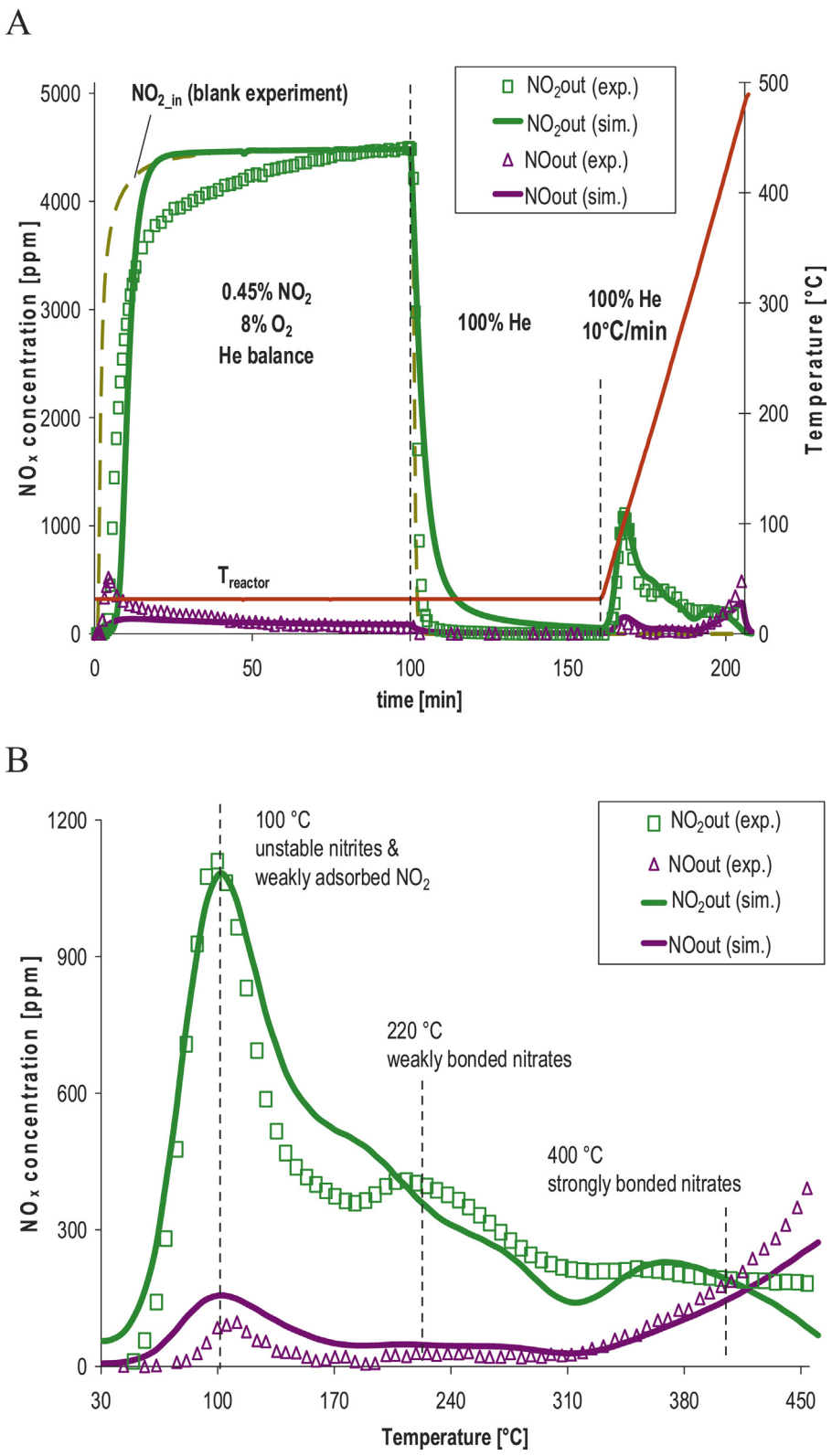

Fig. 6. A) NO_2 adsorption and TPD on the studied H-BEA: Injection of 0.45% NO_2 and 8% O_2 in He, for 100 min at 30 °C, followed by 60 min He flushing at the same temperature and TPD up to 490 °C at a heating rate of 10 °C/min B) Evolution of NO_x as a function of temperature during the TPD phase.

of consumed NO_2 and evolved NO, were estimated equal to 1.44 and 0.64 mol/$kg_{Fe\text{-}BEA}$, respectively, suggesting a stoichiometry of NO_2 disproportionation according to reaction (R.6).

IR spectra recorded during the NO_2/O_2 introduction are collected in Fig. 9 and additional spectral features observed over the Fe-BEA catalyst are summarized in Table 4. Distinguishable IR bands at 1652 and 2133 cm^{-1}, as well as a shoulder at 2175 cm^{-1} were assigned to NO_3^-, NO^+ and N_2O_4/NO^+ (or other species), respectively (Section 4.1.2.1). Further increasing exposure time, besides IR bands characterized over the H-BEA (1865, 1743 and

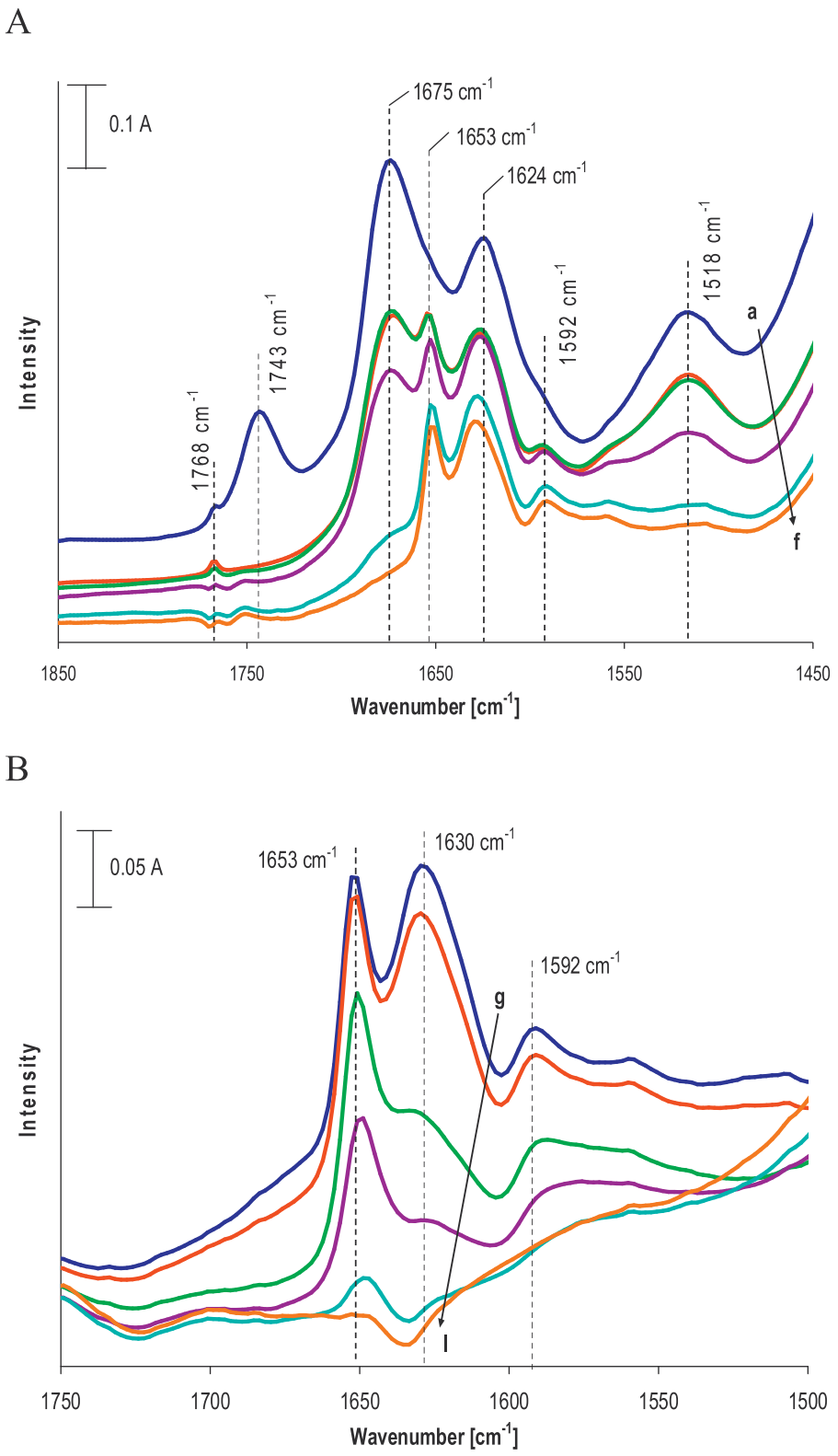

Fig. 7. Difference IR spectra recorded during NO_2-TPD on H-BEA at (a) 30 °C at the end of the NO_2/O_2 injection, (b) 30 °C after 1 h He purging, (c) 50 °C, (d) 75 °C, (e) 100 °C, f) 105 °C, (g) 110 °C, (h) 120 °C, (i) 150 °C, (j) 200 °C, (k) 250 °C, (l) 300 °C.

1592 cm^{-1}) new IR maxima were identified on the Fe-BEA. A band at 1945 cm^{-1} was attributed to NO^+ included in N_2O_4 ($NO^+NO_3^-$) [36], whereas a peak centered at 1633 cm^{-1} was assigned to NO_3 formed on Fe species [12], possibly extra-framework ones [37]. Moreover, the 1517 cm^{-1} band related to NO_2^- shifted to 1527 cm^{-1}.

Evidence of iron based nitrates corresponding to IR bands at 1633 cm^{-1}, tends to indicate that iron can contribute to NO_2

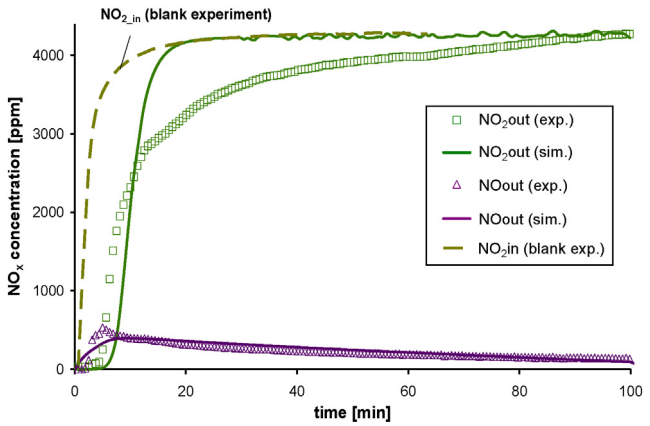

Fig. 8. Gaseous NO_x concentrations recorded during NO_2 storage on the lab-synthesized Fe-BEA zeolite at 30 °C. (Injection of 0.45% NO_2, 8% O_2 and He in balance for 100 min).

Table 4
Summary of additional NO_x adspecies observed during NO_2 adsorption over the Fe-BEA lab-synthesized sample.

Adspecies	IR band (cm^{-1})	References
NO^+ included in N_2O_4	1945	[36]
Bridging Fe based NO_3^-	1633	[12,37]

disproportionation. Iron species existing on the studied Fe-BEA catalyst (mainly Fe^{3+} and Fe binuclear complexes) were previously proved to exhibit Lewis type acidity [18] and hence allow molecular NO_2 adsorption. Therefore, in analogy with the discussion in Section 4.1.2.1, NO_2 disproportionation on the Fe-BEA would lead to the formation of NO_3 coordinated to Fe sites (exhibiting Lewis acidity) and NO^+ on Brønsted sites. Nevertheless, involvement of two metallic adjacent centers for catalyzing NO_2 disproportionation cannot be excluded, since gaseous NO may interact with Fe^{3+} yielding NO^+ and H_2O (Section 4.1.1).

Concerning the nature of iron species, involved in NO_2 adsorption and disproportionation processes, monomeric Fe^{n+}–O^- or Fe^{n+}–OH [12,38], as well as Fe–O–Fe binuclear species [10] have been proposed in the literature. Regarding the latter sites (also termed as α-sites), Dubkov et al. [39] have proved by means of Mössbauer spectroscopy that α-sites constitute binuclear iron complexes composed of two Fe centers, which could be either oxygen bridged by one single oxygen ion O^- (α-oxygen) or equally separately coordinated to one α-oxygen. According to UV-vis spectroscopic measurements over the studied Fe-BEA sample [18], Fe^{3+} isolated cations, iron binuclear complexes and Fe_2O_3 particles were found to coexist on the catalytic surface. Therefore, a contribution of both isolated and binuclear species cannot be excluded.

The thermal stability of the NO_x adspecies formed on the Fe-BEA was examined through the TPD experiment illustrated in Fig. 10. Three desorption peaks clearly appear at 100, 184 and 400 °C. IR spectra recorded during thermo-desorption enabled to correlate adspecies concentration with gaseous concentration signals (Fig. 11). The TPD peak centered at 100 °C was attributed to NO_2 deriving from nitrites (1675 and 1527 cm^{-1}), as well as from weakly adsorbed and/or physisorbed N_2O_4 (1743 cm^{-1}). The second maximum at 184 °C was assigned to NO_2 deriving from bidentate nitrates decomposition (IR band at 1592 cm^{-1}). Evacuating the sample at higher temperatures, the IR maxima at 1653 and 1633 cm^{-1} attenuated but did not vanish, indicating that the NO_2-TPD peak at 400 °C was related to decomposition of strongly coordinated bridging Al- and Fe-based NO_3. Finally, at temperatures higher than 220 °C NO started to evolve in the gas phase (Fig. 10), can be related to NO_2 dissociation.

Collecting information obtained from IR spectroscopic measurements over the H- and Fe-BEA samples it could be suggested that NO_2 can be weakly adsorbed and/or physisorbed, whereas it can adsorbed on acidic sites forming nitrites. Furthermore, NO_2 can chemisorb and disproportionate on framework and extra-framework Al, as well as monomeric and binuclear Fe sites, which could be likely in close vicinity with cationic OH^+ Brønsted acidic ones. Finally, NO_2 can dissociate to NO on FAl and iron sites. These observations are summarized through reactions (R.10) to (R.16).

$$NO_{2(g)} + HO - Si - Z \rightleftharpoons NO_2 - HO - Si - Z \quad \text{(R.10)}$$

$$NO_{2(g)} + T_1 - Z \rightleftharpoons (NO_2 - T_1)^- - Z(T_1 = H^+ \text{and/or} Al) \quad \text{(R.11)}$$

$$2NO_{2(g)} + O - Al_F - Z + 2H^+ - OZ \rightleftharpoons NO_3 - Al_F - Z + NO^+ - Z + HO - H^+ - Z \quad \text{(R.12)}$$

$$2NO_{2(g)} + O - Al_{EF} - Z + 2H^+ - OZ \rightleftharpoons NO_3 - Al_{EF} - Z + NO^+ - Z + HO - H^+ - Z \quad \text{(R.13)}$$

$$2NO_{2(g)} + O - Fe^{3+} - Z + 2H^+ - OZ \rightleftharpoons NO_3 - Fe^{3+} - Z + NO^+ - Z + HO - H^+ - Z \quad \text{(R.14)}$$

$$NO_3 - T_2 - Z \rightleftharpoons NO_{2(g)} + O - T_2 - Z(T_2 = Al_F, Al_{EF}, Fe^{3+}) \quad \text{(R.15)}$$

$$NO_2 - T_3 - Z \rightleftharpoons NO_{(g)} + T_3 - Z(T_3 = Al_F, Fe^{3+}) \quad \text{(R.16)}$$

4.1.3. NO oxidation on Fe-BEA

Finally, NO oxidation over the Fe-BEA catalyst was studied through a stepwise TPD experiment (STPD). Gaseous species concentration profiles are illustrated in Fig. 12. NO oxidation became significant already at 100 °C and reached a maximum yield of 37% at 400 °C. At higher temperatures, the thermodynamic equilibrium shifted towards NO and nitrogen monoxide concentration was stabilized again at 1100 ppm.

IR spectra recorded during the NO oxidation experiment are presented in Fig. 13. Concerning the initial isothermal period at 100 °C (t = 0–60 min), $[Fe\text{-}NO]^{2+}$ mononitrosyls (1872 cm^{-1}), bridging Fe based and monodentate NO_3 (1635 and 1580 cm^{-1} respectively), as well as N_2O_3 (1760 cm^{-1}) were identified (Sections 4.1.1 and 4.1.2). Nitrosium ions (2133 cm^{-1}) were not detected during the NO/O_2 coadsorption experiment. As discussed in Section 4.1.1, nitrosium ions are weakly bonded species, since even at 30 °C they are removed from the surface, after prolonged exposure of the catalyst to NO. Hence, they are reasonably not evidenced during the NO/O_2, coadsorption which is performed at temperatures higher than 100 °C. Upon 20 min of NO/O_2 admission, surface concentration of mononitrosyls started to attenuate and finally the species disappeared after 40 min. Simultaneously, gaseous NO_2 evolved, somehow indicating that NO oxidation initially occurred over Fe sites. Increasing temperature (Fig. 13B) intensities of IR maxima at 1635 and 1580 cm^{-1} decreased, whereas upon 200 °C, recorded IR spectra were no more exploitable. Therefore, it could be concluded that at this temperature range decomposition of NO_3 adspecies formed on Al contributed to the gaseous NO_2 evolution.

Delahay et al. [40] proposed a sequential reaction mechanism, including interaction of the Fe^{2+} ion with O_2 yielding Fe^{3+}–O and

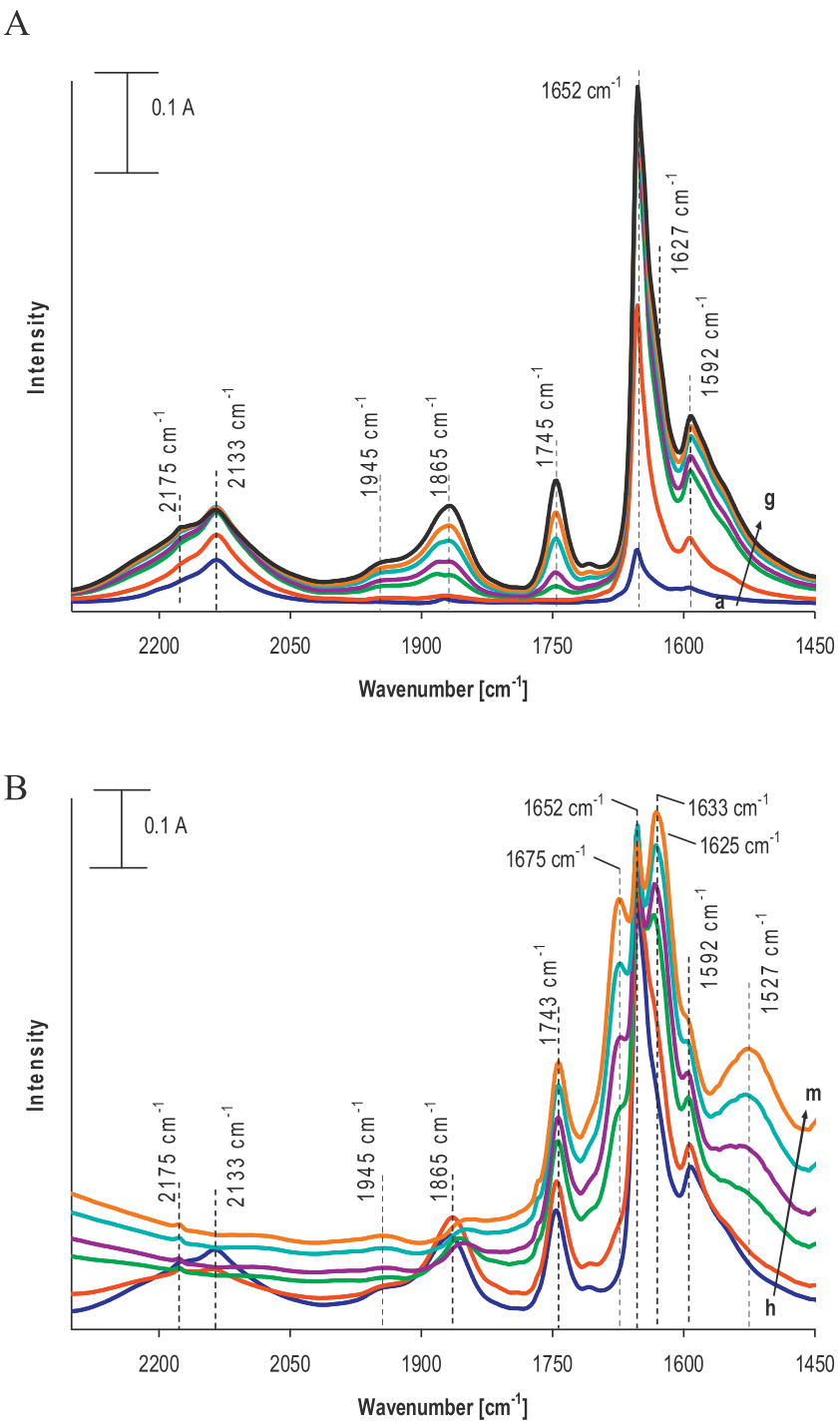

Fig. 9. Difference IR spectra recorded during NO_2 adsorption over the Fe-BEA zeolite at: (a) t = 1.5 min, (b) t = 2 min, (c) t = 3 min, (d) t = 4 min, (e) t = 5 min, (f) t = 7 min, (g) t = 9 min, (h) 10 min, (i) 20 min, (j) 40 min, (k) 60 min, (l) 80 min, (m) 100 min. (Injection of a mixture of 0.43% NO_2 and 8% O_2 diluted in He, at 30 °C, during 100 min).

reaction of the latter with NO towards Fe^{3+}–ONO. The abovementioned mechanism somehow explains the experimental results over the studied Fe-BEA catalyst, since the first 20 min of NO/O_2 adsorption were essential for the catalyst oxidation and/or saturation with oxygen before the oxidation of NO takes place. Therefore, the following redox cycle could be assumed:

$$O_2 + 2Fe^{2+} \rightleftharpoons 2Fe^{3+} - O \quad \text{(R.17)}$$

$$NO_{(g)} + Fe^{3+} - O \rightleftharpoons (Fe - ONO)^{3+} \quad \text{(R.18)}$$

$$Fe^{3+} - ONO \rightleftharpoons Fe^{2+} + NO_2 \quad \text{(R.19)}$$

4.2. Kinetic model for NO_x storage and NO oxidation on Fe-BEA

4.2.1. Multi-site kinetic model development

Based on information obtained through IR spectroscopic measurements, presented in Section 4.1 a multi-site kinetic model for NO_x adsorption/desorption and NO oxidation was developed.

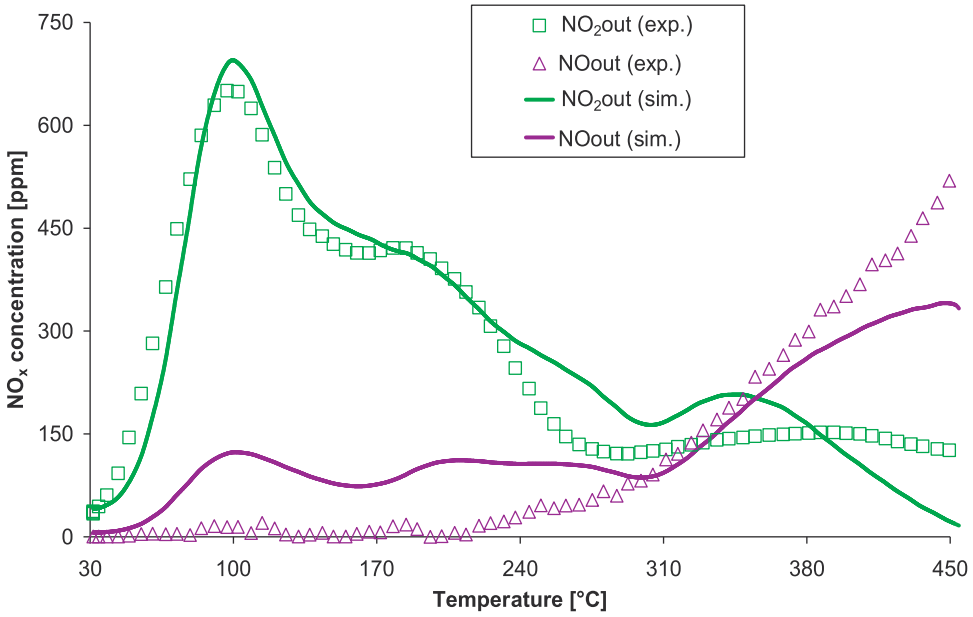

Fig. 10. Gaseous NO_x concentrations recorded during NO_2 TPD on the lab-synthesized Fe-BEA catalyst at 30 °C. (Preadsorption of 0.45% NO_2, 8% O_2 and He in balance at 30 °C for 100 min, followed by 1 h He flushing at the same temperature and TPD up to 490 °C, at a heating rate of 10 °C/min.

Regarding NO adsorption/desorption, only minor quantities were stored over the studied Fe-BEA sample. Therefore, in order to keep the model as simple as possible, NO adsorption/desorption were not modeled. On the other hand, the NO_2 uptake on the H- and Fe-BEA samples was significant and resulted in the formation of various NO_x adspecies. Hence, NO_2 adsorption and disproportionation were modeled in details. Based on the IR band centered at 1743 cm^{-1}, corresponding to weakly adsorbed N_2O_4, we have included a site for weak NO_2 adsorption and/or physisorption, named S1a. Moreover, nitrites formation (1675 and 1518 cm^{-1}) was modeled on a second site, annotated S1b was considered, which was assigned to Brønsted sites. This assumption seemed to be in consistency with the fact that nitrites are generated through oxidation of NO^+, bonded on Brønsted sites (reaction (R.8)).

Modeling of nitrates formation was more complicated. As explained in Section 4.1.2.1, the disproportionation process requires a Lewis and a Brønsted acidic site in close vicinity. Moreover, nitrates can be coordinated in bidentate and bridging configurations involving FAl and EfAl, exhibiting different thermal stability. Therefore, two sites named S2 and S3 were taken into account and were attributed to EfAl and FAl atoms, respectively, located in proximity to cationic OH^+. Regarding NO_2 adsorption and disproportionation on Fe species (Section 4.1.2.2), monomeric iron cations and binuclear Fe species could be involved. Furthermore, NO_2 disproportionation was suggested through synergy of either a pair of two iron sites and/or an iron and a Brønsted site. Nevertheless, since only one type of iron based nitrate was evidenced (1633 cm^{-1}) and in order to keep the model as simple as possible, a single Fe site, named S4 was considered in the proposed mechanism and was related either to a pair of Fe sites or to a pair of a Fe site and a Brønsted type one.

An initial NO_2 adsorption (reaction (R.20)) and a subsequent NO_2 disproportionation (reaction (R.21)) were modeled on S2, S3 and S4 sites in order to depict formation of (i) bidentate NO_3 on EfAl (S2 sites), (ii) bridging NO_3 on FAl and (iii) bridging NO_3 on Fe sites (S4 sites), respectively.

$$NO_{2(g)} \rightleftharpoons NO_{2(ads)} \quad \text{(R.20)}$$

$$2NO_{2(ads)} \rightleftharpoons NO_{3(ads)} + NO_{(g)} \quad \text{(R.21)}$$

Reaction (R.21) implies that nitrates can be decomposed to NO_2 when interacting with gaseous NO. However, as presented in Section 4.1.2, NO_3 was directly decomposed to NO_2 in the presence of He, without involvement of gaseous NO. Therefore, a reversible NO_3 decomposition step was taken into account, yielding surface NO_2 and monatomic oxygen (reaction (R.22)). Adding reactions (R20) to (R.22), reaction (R.6) is found.

$$NO_{2(ads)} + O_{ads} \rightleftharpoons NO_{3(ads)} \quad \text{(R.22)}$$

Since monatomic surface oxygen is required in reaction (R.22), O_2 adsorption and dissociation were modeled on S2, S3, and S4 sites. O_2 adsorption on S1a and S1b sites was purposely not considered, since oxygen does not react with NO_2 on them (even though it could competitively co-adsorb) and the detailed kinetic modeling of O_2 is out of the scope of this study. The multi-site kinetic model for O_2 adsorption and dissociation is illustrated in Table 5, whereas that for NO_2 adsorption and disproportionation in Table 6.

Finally, regarding NO/O_2 co-adsorption on Fe-BEA, Al based acidic and Fe^{3+}–O sites were evidenced to be active for nitrogen monoxide oxidation. Therefore, NO oxidation was modeled on FAl S3 and iron S4 sites (Table 7). Above 400 °C, the thermodynamic equilibrium shifted towards nitrogen monoxide and NO oxidation was hindered (Fig. 12). Moreover, during the NO_2-TPD experiments over the H- and the Fe-BEA and at temperatures above 310 and 220 °C, respectively, NO evolution was observed, due to NO_2 decomposition. Thus, a reversible reaction step was taken into

Table 5
Multi-site kinetic model for O_2 storage on Fe-BEA.

O_2 adsorption on S2 sites[a]	$O_2 + S2 \rightleftharpoons O_2 - S2$
O_2 adsorption on S3 sites[b]	$O_2 + S3 \rightleftharpoons O_2 - S3$
O_2 dissociation on S2 sites[a]	$O_2 + S2 + S2 \rightleftharpoons 2O - S2$
O_2 dissociation on S3 sites[b]	$O_2 + S3 + S3 \rightleftharpoons 2O - S3$
O_2 adsorption on S4 iron based sites[c]	$O_2 + S4 \rightleftharpoons O_2 - S4$
O_2 dissociation on S4 iron based sites[c]	$O_2 + S4 + S4 \rightleftharpoons 2O - S4$

[a] S2 sites represent a pair of an Al based Lewis site and a Si–OH^+–Al Brønsted one, where bidentate NO_3^- can be formed.
[b] S3 sites represent a pair of an Al based Lewis site and a Si–OH^+–Al Brønsted one, where bridging NO_3^- can be formed.
[c] S4 sites represent a pair of an isolated or binuclear iron site in the Fe^{3+} state and a Si–OH^+–Al Brønsted and/or a second metallic one.

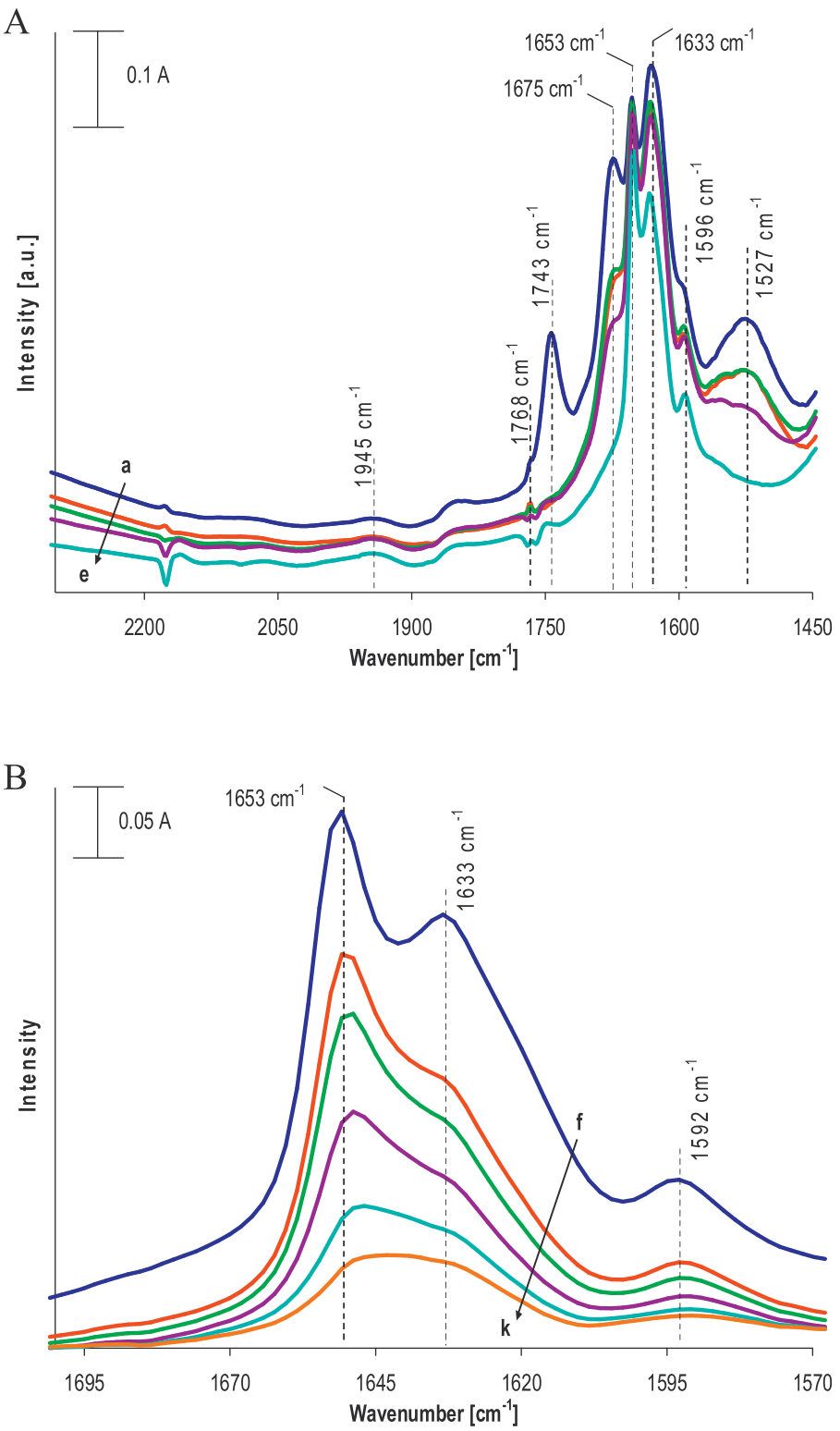

Fig. 11. Difference IR spectra recorded during NO_2-TPD on Fe-BEA at (a) 30 °C at the end of the NO_2/O_2 injection, (b) 30 °C after 1 h He purging, (c) 50 °C, (d) 75 °C, (e) 100 °C, (f) 115 °C, (g) 150 °C, (h) 170 °C, (i) 190 °C, (j) 210 °C, (k) 220 °C.

account, corresponding to NO_2 dissociation. The S3 site was purposely chosen for modeling NO oxidation instead of the S2 one. NO_3 formed on FAl (S3 site) is thermally stable at temperatures as high as 300 °C, which means that NO_2 dissociation taking place in this temperature range possibly occurs on the same site. Reaction rate expressions applied for the proposed multi-site kinetic model are summarized in Table S1 (Supplementary Material).

4.2.2. Simulation of NO_2 adsorption and desorption experiments

4.2.2.1. Simulation of experiments over the lab-synthesized H- and Fe-BEA samples. The kinetic model was initially used for simulating the NO_2 adsorption and TPD experiments performed on the studied H- and Fe-BEA presented in Section 4.1.2. For simulation purposes the single wafer reactor model was used. Special care was taken for determining model kinetic parameters. A detailed description

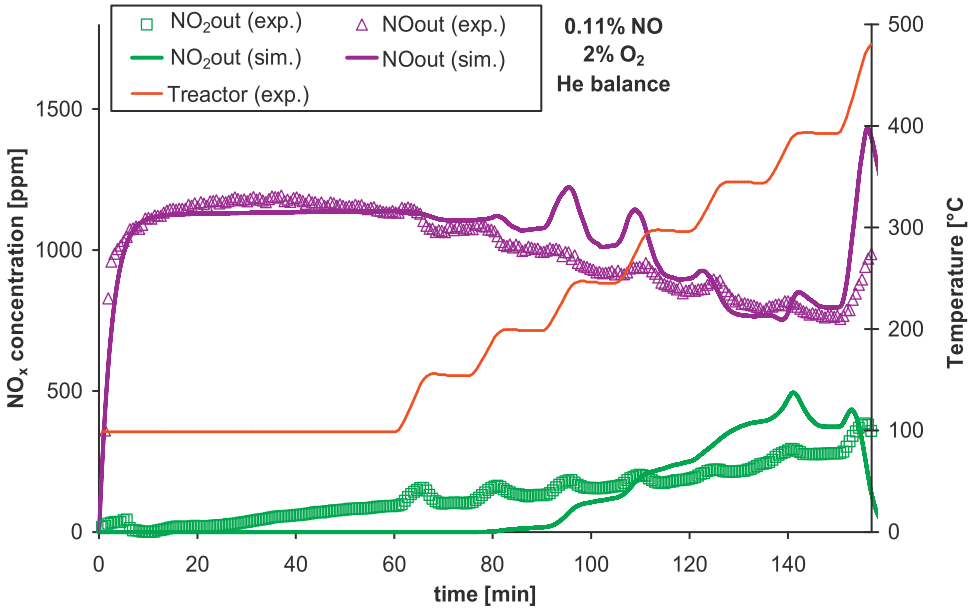

Fig. 12. Gaseous NO_x concentrations recorded during NO oxidation experiment (Injection of a mixture of 1100 ppm NO and 2% O_2 diluted in He and stepwise TPD from 100 to 480 °C).

Table 6
Kinetic model for NO_2 storage and disproportionation on Fe-BEA.

NO_2 adsorption on S1a non acidic sites	$NO_2 + S1a \rightleftharpoons NO_2 - S1a$
NO_2^- formation on S1b Brønsted sites	$NO_2 + S1b \rightleftharpoons NO_2 - S1b$
NO_2 adsorption on S2 sites[a]	$NO_2 + S2 \rightleftharpoons NO_2 - S2$
NO_2 adsorption on S3 sites[b]	$NO_2 + S3 \rightleftharpoons NO_2 - S3$
NO_2 adsorption on S4 sites[c]	$NO_2 + S4 \rightleftharpoons NO_2 - S4$
NO_2 disproportionation on S2 sites[a]	$2NO_2 - S2 \rightleftharpoons NO_3 - S2 + NO_{(g)} + S2$
	$NO_2 - S2 + O - S2 \rightleftharpoons NO_3 - S2 + S2$
NO_2 disproportionation on S3 sites[b]	$2NO_2 - S3 \rightleftharpoons NO_3 - S3 + NO_{(g)} + S3$
	$NO_2 - S3 + O - S3 \rightleftharpoons NO_3 - S3 + S3$
NO_2 disproportionation on S4 sites[c]	$2NO_2 - S4 \rightleftharpoons NO_3 - S4 + NO_{(g)} + S4$
	$NO_2 - S4 + O - S4 \rightleftharpoons NO_3 - S4 + S4$

[a] S2 sites represent a pair of an Al based Lewis site and a Si–OH^+–Al Brønsted one, where bidentate NO_3^- can be formed.
[b] S3 sites represent a pair of an Al based Lewis site and a Si–OH^+–Al Brønsted one, where bridging NO_3^- can be formed.
[c] S4 sites represent a pair of an isolated or binuclear iron site in the Fe^{3+} state and a Si–OH^+–Al Brønsted and/or a second metallic one.

of kinetics calibration is presented in the Supplementary Material section (see Tables S2 to S8).

Regarding NO_2/O_2 storage and release over H-BEA, simulation results are illustrated in Figs. 3 and 6. The proposed kinetic model reproduced the tendency of the experimental curves during both the adsorption and TPD phases. Considering the first 100 min, NO_2 adsorption as well as NO evolution, according to reactions (R.20) to (R.22) were simulated, resulting in a relatively acceptable reproduction of the experimental curves (Fig. 3). Nevertheless, the NO maximum concentration originating from NO_2 disproportionation was underestimated. Furthermore, the NO_2 simulated concentration signal was stabilized to the injected concentration of 0.45% at around 17 min upon surface saturation, whereas the respective experimental one after 80 min. These discrepancies could be attributed to several reasons. First of all, the proposed kinetic model accounted only for a two step mechanism including NO_2 adsorption and a subsequent disproportionation, whereas interactions between NO and NO_2 (e.g. formation of N_2O_3 and N_2O_4) were not taken into consideration for simplicity purposes. Moreover, reviewing the studies according to which kinetic parameters were obtained it appears that the set of parameters proposed in this work was mainly validated for NO_2 adsorption experiments performed at higher temperatures. Finally, limitations of the single wafer reactor model cannot be ruled out, since the reactor was modeled as a 0-D CSTR. As far as the TPD phase is concerned, three distinguishable desorption peaks, centered at around 100, 220 and 370 °C were correctly simulated, whereas above 310 °C, NO evolution due to NO_2 dissociation (backward step of reaction (R.18)) was satisfactorily depicted. Before simulating the TPD experiment, the contribution of each model site was simulated separately (Fig. S3 in Supplementary Material). In accordance with the IR spectroscopy measurements presented in Section 4.1.2.1, weakly adsorbed and/or physisorbed NO_2 on S1a sites, as well as nitrites on S1b Brønsted acidic sites were responsible for the NO_2-TPD peak centered at around 100 °C. Moreover, NO_2 originating from decomposition of bidentate and bridging NO_3 formed on S2 and S3 sites, respectively, reproduced the thermo-desorption peaks lying at 220 and 380 °C.

Table 7
Multi-site kinetic model for NO oxidation.

NO oxidation on S3 sites[a]	$NO_{(g)} + O - S3 \rightleftharpoons NO_2 - S3$
NO oxidation on S4 sites[b]	$NO_{(g)} + O - S4 \rightleftharpoons NO_2 - S$

[a] S3 sites represent a pair of an Al based Lewis site and a Si–OH^+–Al Brønsted one.
[b] S4 sites represent a pair of an isolated or binuclear iron site in the Fe^{3+} state and a Si–OH^+–Al Brønsted and/or a second metallic one.

Comparison between simulation and experimental data for NO_2/O_2 storage and release over the Fe-BEA sample are presented in Figs. 8 and 10. The multi-site kinetic model led to relatively satisfactory simulations, enabling to depict the tendency of the experimental data. In the case of the Fe exchanged catalyst, NO evolution upon surface saturation with NO_2/O_2 was somehow correctly simulated, due to the additional contribution of the S4 metallic site. Focusing on the TPD experiment, the multi-site kinetic model succeeded in simulating gaseous NO_2 evolution originating from the decomposition of nitrites as well as Al and Fe based nitrates, in line with experimental results obtained from IR spectroscopic measurements. Finally, NO_2 dissociation was predicted at temperatures higher than 200 °C. However, an overestimation of the NO concentration is observable within the range of 100–310 °C, which may be attributed either to the fact that the NO storage was not modeled, or to the simplified reactions scheme applied.

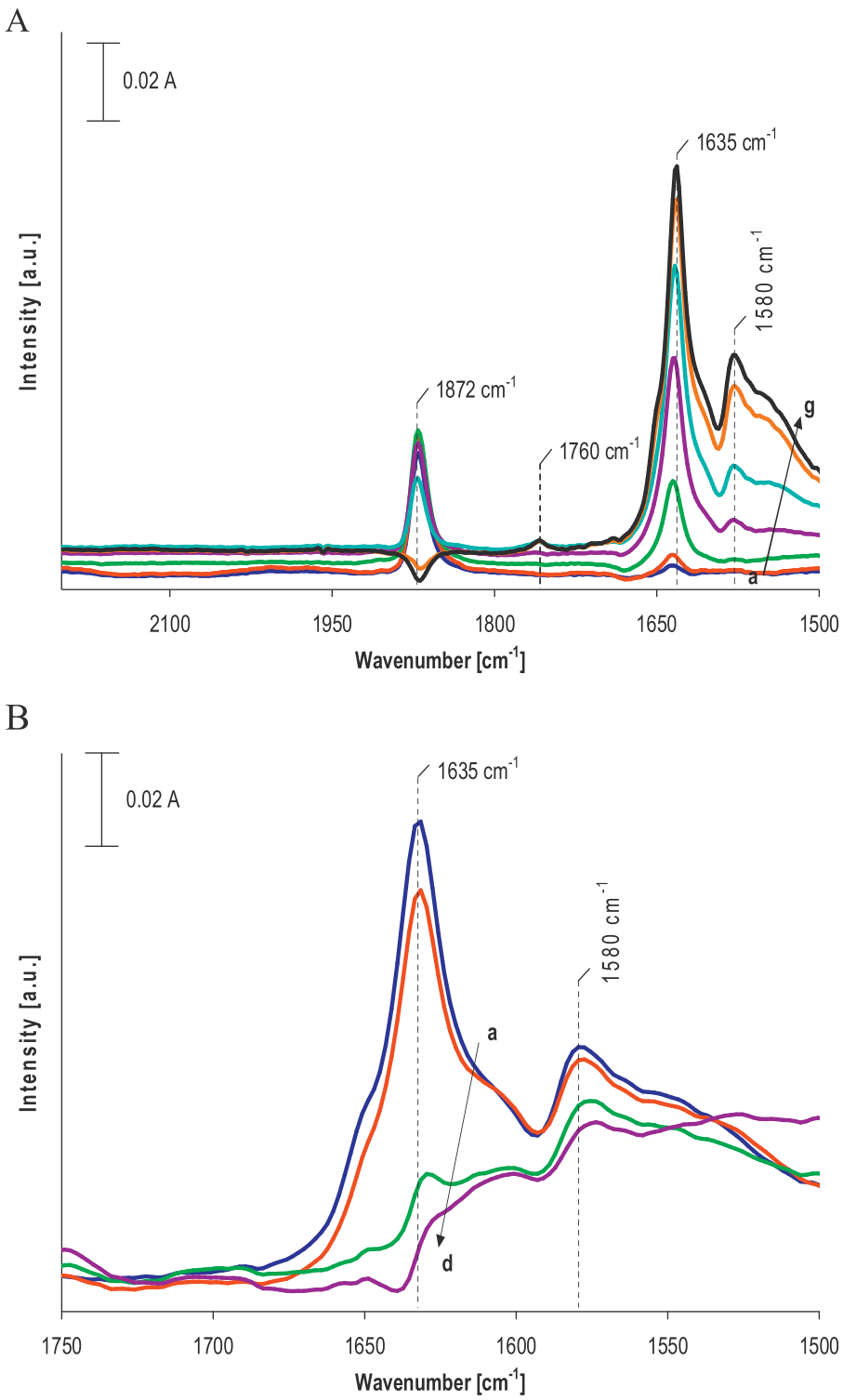

Fig. 13. Difference IR spectra recorded during the NO oxidation experiment. (A) Spectra recorded at (a) 1 min, (b) 2 min, (c) 5 min, (d) 10 min, (e) 20 min, (f) 40 min and (g) 60 min, (B) Spectra recorded at (a) 100 °C, (b) 145 °C, (c) 155 °C and (d) 200 °C.

4.2.2.2. Simulation of experiments over a commercial Fe-BEA catalyst. The proposed multi-site kinetic model was further evaluated over a commercial Fe-BEA catalyst, reported by Colombo et al. [9]. Two NO_2 adsorption and TPD experiments were performed on a commercial, oxidized Fe-BEA catalyst (SAR = 24, Fe/Al = 1.5). During the first test case, 1000 ppm NO_2, diluted in He were preadsorbed at 200 °C, for 500 min, followed by a TPD up to 500 °C, at a heating rate of 10 °C/min. The same protocol was applied for the second experiment. Though, in this case, the catalyst was exposed to a mixture of 1000 ppm NO_2, 2% O_2, and He in balance prior to the TPD run. Both experiments were performed on a fixed bed reactor [9] and thus the respective reactor model was used for simulation purposes. The kinetic model had to be recalibrated to correctly depict experimental data. A single set of kinetic parameters, collected in Tables S9 to S15 (Supplementary Material), was used for simulating both experiments. Kinetics recalibration was

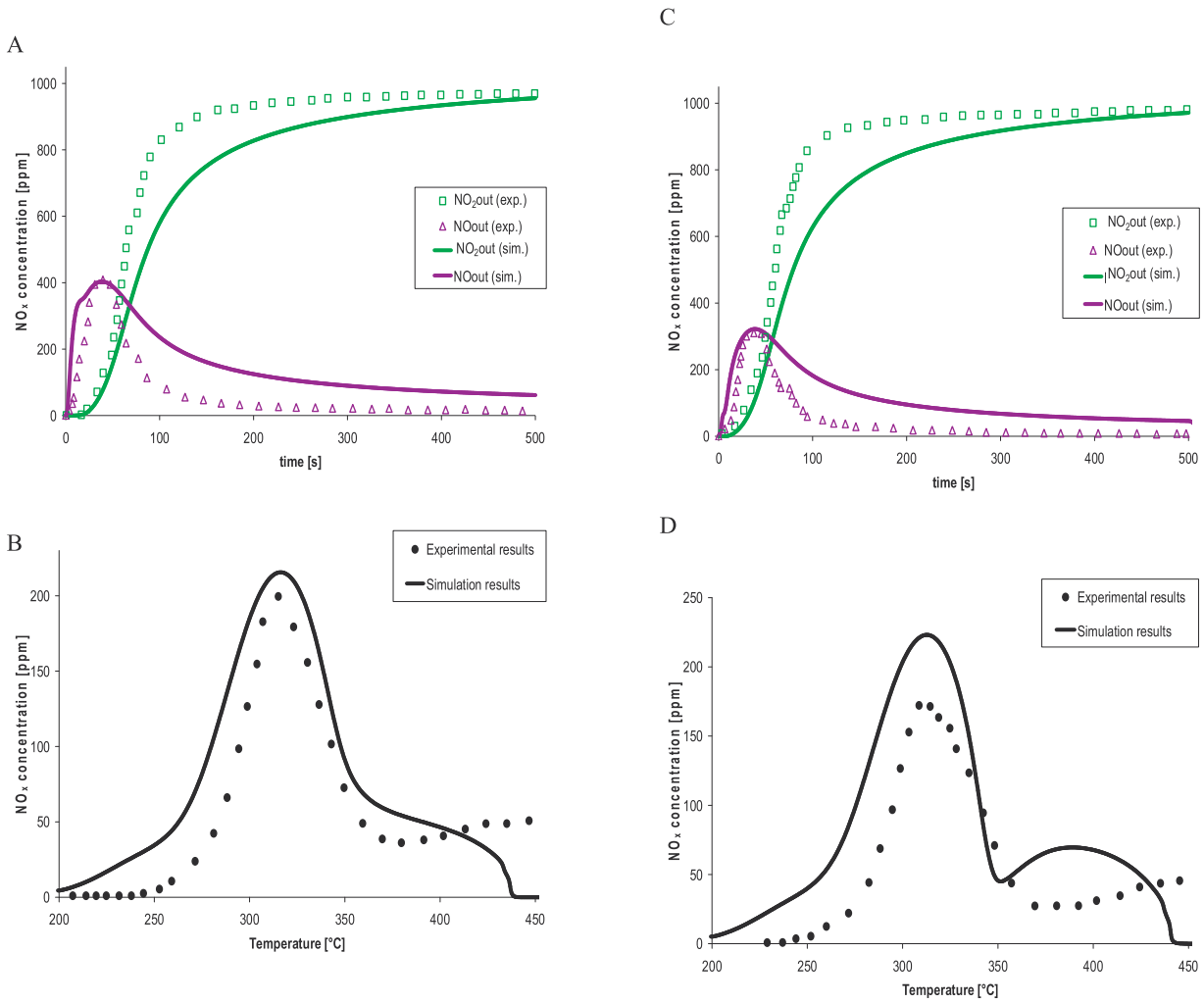

Fig. 14. Simulation of NO_2 adsorption and TPD experiment over a commercial Fe-BEA catalyst, reported by Colombo et al. [9]. Preadsorption of 1000 ppm NO_2 diluted in He (Fig. A) and 1000 ppm NO_2, 2% O_2 and He in balance (Fig. C) at 200 °C for 500 s, followed by a TPD performed from 200 to 500 °C, at 10 °C/min under He (Figs. B and D).

somehow expected because: a) the Si/Al ratio of the commercial sample was higher compared to the lab-synthesized Fe-BEA. As discussed in Section 4.1.2, the distribution of FAl and EfAl is crucial for NO_2 disproportionation, since they constitute the active sites for NO_3 formation. Moreover, the synthesis method (including catalyst post-treatment: e.g. calcination) is unknown and thus the nature of iron species and the state of the zeolite cannot be concluded.

Experimental and simulation NO_x gaseous profiles are illustrated in Fig. 14 A to D. Concerning the adsorption phase (Fig. 14A and C) NO_2 storage and NO evolution were correctly simulated for both experiments. Colombo et al. [9] reported that the ratio between consumed NO_2 and evolved NO was ca 0.38–0.45, which seems to validate experimental results obtained over the lab-synthesized Fe-BEA catalyst (Section 4.1.2.2). Interestingly, NO production was predicted quite precisely, which tends to validate the fact that proposed kinetic parameters might be suitable mainly for NO_2 adsorption experiments performed at this temperature range (200 °C). It is noteworthy that competitive adsorption between NO_2 and O_2 was correctly depicted. Indeed, in the NO_2/He adsorption case, a maximum NO concentration of 409 ppm was simulated, whereas for the NO_2/O_2/He adsorption experiment a NO maximum of ca 315 ppm was computed.

Regarding the TPD phase (Fig. 14B and D), a distinguishable NO_x desorption peak centered at 310 °C, as well as a shoulder lying within the temperature range of 350–450 °C were observed, which according to Colombo et al. [9] were assigned to NO_2 deriving from decomposition of NO_3 previously formed on metallic and zeolitic acidic sites, respectively. According to IR spectroscopic measurements obtained over the Fe-BEA lab-synthesized sample (Section 4.1.2.2) it could be speculated that the high temperature NO_2 shoulder could be assigned to decomposition of FAl based bridging NO_3. Considering this analysis, S4 and S3 model sites simulated NO_x-TPD peaks at 310 and 400 °C, respectively, highlighting the contribution of Fe and the zeolitic support of this commercial catalyst to NO_2 adsorption and disproportionation reaction steps.

Interestingly, for the experimental case where NO_2/O_2/He were preadsorbed, the TPD peak at 310 °C attenuated from 200 to 173 ppm, which was not predicted by the kinetic model. This discrepancy could be attributed to: a) experiment reproducibility issues, since the difference between the maximum NO_x concentration is less than 30 ppm and/or b) the simulation of compensating reactions. Regarding the latter, the model depicted competitive adsorption between NO_2 and O_2, which could lead to a lower NO_2 uptake. Consequently a lower amount of NO_3 is formed (reactions (R.20) and (R.21)). Nevertheless, when O_2 coexist in the feed, reaction (R.22) is also activated, which could increase the amount of stored nitrate adspecies.

In order to understand the predominant reaction pathways for NO_3 formation, a kinetic parameters sensitivity analysis with

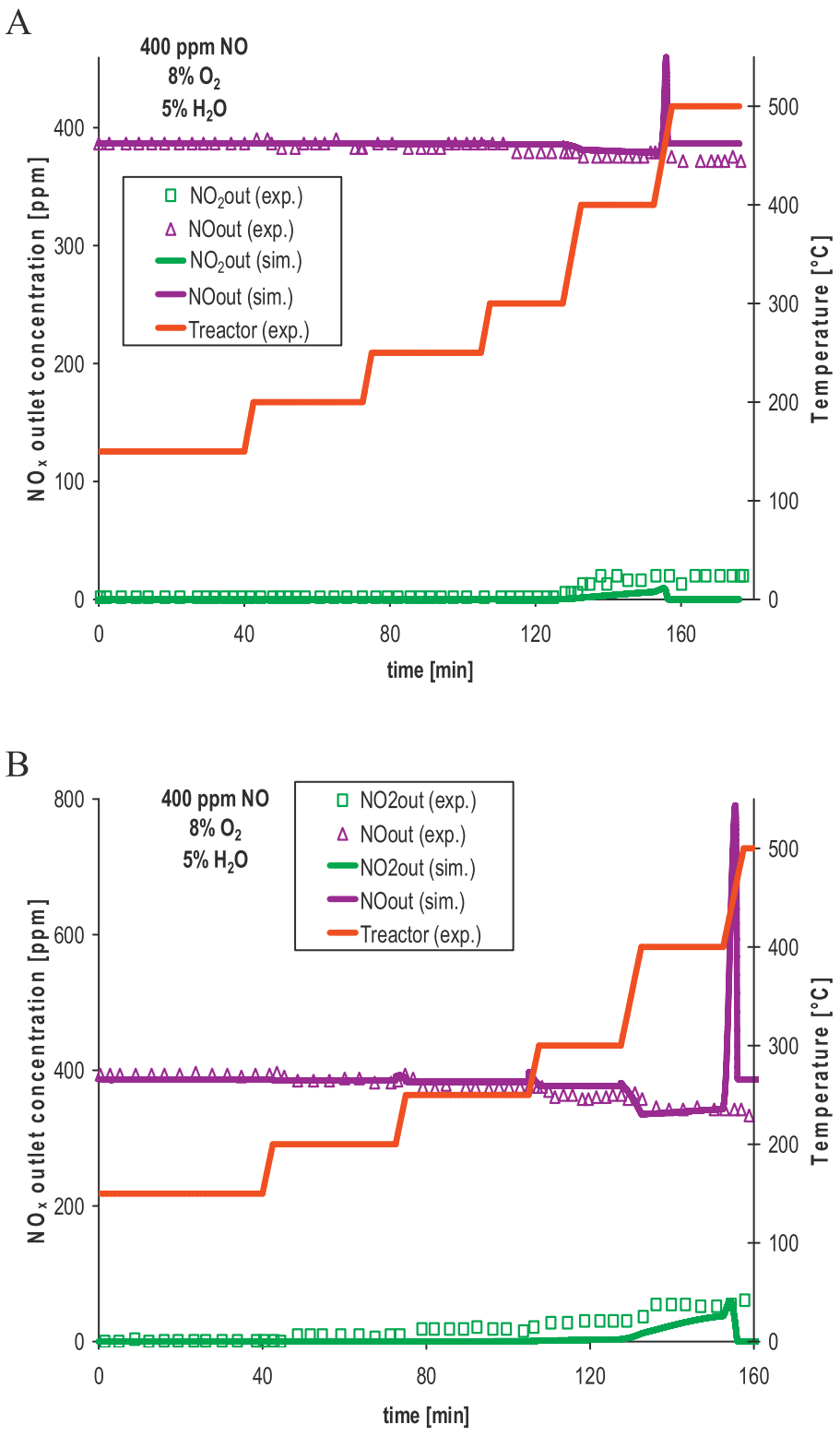

Fig. 15. Simulation of a NO/O_2 STPD experiment over a (A) H- and a (B) Fe-BEA sample, reported by Shwan et al. [11]. Continuous injection of a mixture of a 400 ppm NO, 8% O_2 and 5% H_2O mixture diluted in Ar.

respect to the S4 site was performed for the abovementioned NO_2/O_2 adsorption and TPD experiment over the commercial Fe-BEA. More information concerning the performance of a sensitivity analysis can be found elsewhere [41]. As clearly shown in Fig. S4 (Supplementary Material) oxygen adsorption and dissociation, as well as NO_2 disproportionation are the predominant steps, which control NO production upon surface saturation with NO_2/O_2. As explained, NO evolution due to NO_2 disproportionation is hindered when O_2 is in the feed, due to NO_2/O_2 competitive adsorption. On the other hand, NO_2 release at 310 °C, related to decomposition of Fe based NO_3 is reasonably governed by NO_2 adsorption and disproportionation (reactions (R.20) and (R.21)). As it was suggested, when the Fe-BEA is exposed to a NO_2/O_2 mixture reaction (R.22) is also activated, leading to the formation of additional amounts of

NO_3. Hence, the assumption for compensating reaction steps seems to be validated.

4.2.3. Simulation of NO oxidation experiments

NO oxidation experiments were subsequently simulated. The NO/O_2 STPD experiment performed over the lab-synthesized Fe-BEA catalyst (Section 4.1.3) was simulated first. Kinetic parameters used were the same with those applied for simulating the NO_2/O_2 adsorption and TPD experiments over the same catalytic sample (Supplementary Material/Tables S2 to S8), without any modification. Computed results, shown in Fig. 12 seem to follow the tendency of the experimental curves, especially within the 250–400 °C range. Interestingly, the kinetic model did not succeed in depicting NO oxidation at temperatures lower than 200 °C. Olsson et al. [16] similarly observed low temperature nitrogen monoxide oxidation over a Cu-ZSM5 (SiO_2/Al_2O_3 = 27, 2.03 wt.% Cu). These authors suggested NO oxidation over non acidic sites and subsequently modeled the abovementioned phenomenon, which allowed obtaining satisfactory simulation results. Nevertheless, according to IR spectroscopic measurements presented in Section 4.1.3, only metallic and acidic sites were evidenced to catalyze NO oxidation. According to UV–vis spectroscopy measurements over the studied Fe-BEA [18] isolated as well as binuclear iron species co-exist the lab-synthesized Fe-BEA catalyst. Thus, it was supposed that there is more than one type of iron sites contributing to NO oxidation. However, in order to keep model complexity in reasonable extents it was decided to account for a single global Fe model site. At temperatures higher than 400 °C, NO concentration increased, converging to 1100 ppm, in accordance with the NO_2/NO thermodynamic equilibrium discussed in Section 4.1.3. An overestimation of NO concentration was observed during the heating phase and at temperatures higher than 400 °C and could be related to the fact that NO storage modeling was neglected in our kinetic model.

Two additional NO/O_2 STPD experiments performed over H- and a Fe-BEA samples, reported by Shwan et al. [11] were also simulated. A H-BEA zeolite (SAR = 38) and a 1 wt.% Fe-BEA catalyst, loaded on a monolith reactor were exposed to a mixture of 400 ppm NO, 8% O_2 and 5% H_2O, with Ar in balance, whereas temperature was stepwisely increased from 150 to 500 °C. For simulation purposes the monolith reactor model was used. Comparison between computed and experimental results is illustrated in Fig. 15. For these test cases, kinetic parameters previously applied for the lab-synthesized H- and Fe-BEA samples (Supplementary Material/Tables S2 to S8) were used. Only the oxygen desorption activation energy over S4 metallic sites had to be calibrated to 40 instead of 48 kJ/mol in order to correctly fit experimental curves. The H-BEA reported by Shwan et al. [11] has similar Al content, compared to our lab-synthesized BEA zeolite, whereas wet ion exchange was the method used for synthesizing the Fe-BEA catalyst in both cases. These observations may explain why in this case similar kinetics could be applied.

Simulation results are in good agreement with experimental ones, indicating that the proposed set of kinetic parameters could constitute a quite reliable data base for the kinetic modeling of NO_x adsorption and NO oxidation over H- and Fe-BEA with similar structural properties. Results clearly prove the contribution of acidic and metallic sites to NO oxidation, in line with IR spectroscopic measurements (Section 4.1.3). NO gaseous concentration signal was overestimated for temperatures higher than 400 °C, which may be attributed to the fact NO storage was not modeled.

5. Conclusions

A detailed IR spectroscopy study over H- and Fe-BEA lab-synthesized samples was performed in order to develop a multi-site kinetic model for NO_x storage and NO oxidation over Fe exchanged BEA catalysts. Analysis of NO adsorption/desorption experiments proved that only minor amounts of NO were admitted on monomeric Fe^{2+}, cationic OH^+ and extra-framework Al–OH sites. On the other hand, surface nitrites, nitrates, as well as gaseous NO evolution were observed upon NO_2 adsorption and disproportionation. The latter reaction was proved to occur on cationic OH^+ and Al and Fe sites located in neighboring positions. Nitrites, as well as physisorbed and/or weakly adsorbed NO_2 were the predominant surface species at temperatures up to 100 °C, whereas NO_3 were found to be stable at higher ones. Three different types of nitrate adspecies were identified, including bidentate and bridging NO_3 coordinated on extra-framework and framework Al, respectively, as well as bridging nitrates formed on oxidized monomeric and/or binuclear iron sites. Finally, as far as NO oxidation is concerned, zeolitic aluminum and Fe^{3+}–O were found to be the respective active sites.

Compiling information obtained through IR spectroscopic measurements, a multi-site kinetic model for NO_x storage and NO oxidation was developed. Five surface sites were considered, including a site for physisorption and/or weak adsorption, as well as a Brønsted site for nitrites formation. Moreover, in order to precisely depict bidentate and tridentate nitrates coordinated to Al, two additional sites were considered, being assigned to pairs of $EFAl/OH^+$ and FAl/OH^+. Finally, NO_3 formation on metallic sites was modeled by adopting a global Fe site, which was assigned to either a pair of two isolated and/or binuclear Fe^{3+} species or a pair of Fe^{3+}/OH^+. NO_2 adsorption and disproportionation, O_2 storage and dissociation, as well as NO oxidation and NO_2 dissociation were modeled over the abovementioned sites, whereas NO adsorption/desorption were neglected.

The proposed kinetic model succeeded in reproducing experimental results, obtained over the lab-synthesized H- and Fe-BEA samples, as well as catalytic samples reported in the literature. Interestingly, switching between different Fe-BEA samples, the model had to be recalibrated in order to correctly simulate experimental data. Indeed, kinetic parameters are directly related to structural properties of the catalyst (e.g., Al and Fe content) which may imply that the kinetic model could be applied for different types of Fe-exchanged zeolites, besides Fe-BEA. Overall, the multi-site kinetic modeling approach succeeded in depicting the contribution of acidic and metallic sites to NO_x adspecies formation and NO oxidation, which highlights the interest of the methodology used.

It is noteworthy that in all experiments, presented in this work, dry conditions were applied. Nevertheless, water is a major compound of diesel engines exhaust stream. It is extensively reported that H_2O significantly affects NO_x adsorption and NO to NO_2 oxidation. For instance, in-situ IR spectroscopic measurements of NO_2 adsorption in the presence of H_2O, earlier presented by Ahrens et al. [12], tend to support interactions of nitrogen dioxide with water towards HNO_2 and HNO_3. The latter compound was evidenced through IR maxima centred at 1675, 1404 and 1312 cm^{-1}. For the scope of the herein study, water was purposely neglected, since the presence of surface H_2O species can be easily detected through IR spectroscopy, disturbing the spectral interpretation [42]. Spectroscopic analysis and kinetic modeling of such aspects could be considered for future work.

Acknowledgements

Mr. J. C. Morin is also kindly acknowledged for his contribution to the experimental part. Moreover, Drs N. Bats and N. Rankovic are also thanked for providing the H-BEA parent zeolite and performing calculations in Dmol, respectively.

Appendix A. Supplementary data

Supplementary material related to this article can be found, in the online version, at http://dx.doi.org/10.1016/j.apcatb.2013.11.018.

References

[1] R. Nedyalkova, S. Shwan, M. Skoglundh, L. Olsson, Appl. Catal., B 138–39 (2013) 373–380.
[2] J.M. Fedeyko, US Patent 0 250 127, 2011, to Johnson Matthey Public Limited Company.
[3] P. Granger, V.I. Parvulescu, Chem. Rev. 111 (2011) 3155–3207.
[4] S. Brandenberger, O. Kröcher, A. Tissler, R. Althoff, Catal. Rev. 50 (2008) 492–531.
[5] A. Grossale, I. Nova, E. Tronconi, D. Chatterjee, M. Weibel, Top. Catal. 52 (2009) 1837–1841.
[6] A. Grossale, I. Nova, E. Tronconi, D. Chatterjee, M. Weibel, J. Catal. 256 (2008) 312.
[7] A. Grossale, I. Nova, E. Tronconi, Catal. Lett. 130 (2009) 525–531.
[8] M.P. Ruggeri, I. Nova, E. Tronconi, Top. Catal 56 (2013) 109–113.
[9] M. Colombo, I. Nova, E. Tronconi, Appl. Catal., B 111–112 (2012) 433–444.
[10] M. Iwasaki, H. Shinjoh, J. Catal. 273 (2010) 29–38.
[11] S. Shwan, J. Jansson, J. Korsgren, L. Olsson, M. Skoglundh, Catal. Today 197 (2012) 24–37.
[12] M. Ahrens, O. Marie, P. Bazin, M. Daturi, J. Catal. 271 (2010) 1–11.
[13] R. Kefirov, E. Ivanova, K. Hadjiivanov, S. Dzwigaj, M. Che, Catal. Lett. 125 (2008) 209–214.
[14] P.S. Metkar, V. Balakotaiah, M.P. Harold, Catal. Today 184 (2012) 115–128.
[15] V. Bacher, C. Perbandt, M. Schwefer, R. Siefert, T. Turek, Appl. Catal., B 134–135 (2013) 55–59.
[16] L. Olsson, H. Sjövall, R.J. Blint, Appl. Catal., B 87 (2009) 200–210.
[17] M. Colombo, I. Nova, E. Tronconi, Catal. Today 197 (2012) 243–255.
[18] S.A. Skarlis, D. Berthout, A. Nicolle, C. Dujardin, P. Granger, J. Phys. Chem. C 117 (2013) 7154–7169.
[19] G. Mauviot, F. Le Berr, S. Raux, F. Perretti, L. Malbec, C. Millet, Oil & Gas Science and Technology—Rev. IFP 64 (2009) 285–307.
[20] S.A. Skarlis, D. Berthout, A. Nicolle, C. Dujardin, P. Granger, J. Phys. Chem. C 116 (2012) 8437–8448.
[21] K. Leistner, A. Nicolle, D. Berthout, P. Da Costa, Combust. Flame 159 (2012) 64–76.
[22] S.A. Skarlis, D. Berthout, A. Nicolle, C. Dujardin, P. Granger, Procedia—Social Behav. Sci. 48 (2012) 1672–1682.
[23] K. Hadjiivanov, J. Saussey, J.L. Freysz, J.C. Lavalley, Catal. Lett. 52 (1998) 103–108.
[24] K.I. Hadjiivanov, Catal. Rev. 42 (2000) 71–144.
[25] C. Sedlmair, B. Gil, K. Seshan, A. Jentys, J.A. Lercher, Phys. Chem. Chem. Phys. 5 (2003) 1897–1905.
[26] I. Perdana, D. Creaser, O. Öhrman, J. Hedlund, J. Catal. 234 (2005) 219–229.
[27] J. Szanyi, M.T. Paffett, J. Catal. 164 (1996) 232–245.
[28] R. Brosius, P. Bazin, F. Thibault-Starzyk, J.A. Martens, J. Catal. 234 (2005) 191–198.
[29] L. Lobree, I. Hwang, J. Reimer, A. Bell, Catal. Lett. 63 (1999) 233–240.
[30] I. Nova, C. Ciardelli, E. Tronconi, D. Chatterjee, B. Bandl-Konrad, Catal. Today 114 (2006) 3–12.
[31] A.L. Goodman, G.M. Underwood, V.H. Grassian, J. Phys. Chem. A 103 (1999) 7217–7223.
[32] N. Apostolescu, T. Schröder, S. Kureti, Appl. Catal., B 51 (2004) 43–50.
[33] Z.M. Wang, T. Arai, M. Kumagai, Ind. Eng. Chem. Res. 40 (2001) 1864–1871.
[34] E.A. Pidko, P. Mignon, P. Geerlings, R.A. Schoonheydt, R.A. van Santen, J. Phys. Chem. C 112 (2008) 5510–5519.
[35] P. Mignon, E.A. Pidko, R.A. Van Santen, P. Geerlings, R.A. Schoonheydt, Chem.Eur. J. 14 (2008) 5168–5177.
[36] K. Hensel, M. Morvová, Contrib. Plasma Phys. 36 (1996) 51–61.
[37] G. Mul, J. Pérez-Ramírez, F. Kapteijn, J.A. Moulijn, Catal. Lett. 80 (2002) 129–138.
[38] M.P. Ruggeri, A. Grossale, I. Nova, E. Tronconi, H. Jirglova, Z. Sobalik, Catal. Today 184 (2012) 107–114.
[39] K.A. Dubkov, N.S. Ovanesyan, A.A. Shteinman, E.V. Starokon, G.I. Panov, J. Catal. 207 (2002) 341–352.
[40] G. Delahay, D. Valade, A. Guzmán-Vargas, B. Coq, Appl. Catal., B 55 (2005) 149–155.
[41] D. Mantri, P. Aghalayam, Catal. Today 119 (2007) 88–93.
[42] A. Vimont, F. Thibault-Starzyk, M. Daturi, Chem. Soc. Rev. 39 (2010) 4928–4950.